Bureau of Mineral Resources, Geology & Geophysics

R E C O R D

RECORD 1990 / 38

Chemical Modelling of Lead - Zinc Transport and Deposition in Mississippi Valley-Type Deposits of the Lennard Shelf, Canning Basin, Western Australia.

by

Subhash Jaireth , Hashem Etminan, and Christoph A. Heinrich

1990/38
COPY 4

BUREAU OF MINERAL RESOURCES
GEOLOGY AND GEOPHYSICS

RECORD 1990 / 38

Chemical Modelling of Lead - Zinc Transport and Deposition in Mississippi Valley-Type Deposits of the Lennard Shelf, Canning Basin, Western Australia.

by

Subhash Jaireth*, Hashem Etminan, and Christoph A. Heinrich

*now at Geology Department, James Cook University of N. Queensland, Townsville

Contents

Acknowledgements

Subhash Jaireth would like to thank the Baas Becking Geobiological Laboratory for financial assistance to carry out this study. He would also like to thank the Ministry of Human Resources Development, Government of India for awarding him a National Fellowship to undertake research at the Bureau of Mineral Resources, Canberra. We would all like to acknowledge the fruitful interaction with BHP-Utah and Billiton Ltd, who provided unpublished company information about the deposits. We are grateful to M.Solomon, J.Ferguson and G.Ewers for helpful discussions and comments during this study.

Abstract

Chemical models for the formation of Mississippi Valley Type (MVT) deposits are faced with the problem of relatively low solubilities of galena and sphalerite at the typically quite low formation temperatures of these deposits. Transport of reduced sulphur and metals in two separated fluids has been proposed to solve the chemical problem, but faces the physical problem of mixing large amounts of subsurface fluids. Moreover, many MVT deposits including those on the Lennard Shelf of the Canning Basin lack geological evidence for fluid mixing.

This report presents a review of geological observations on the Canning Basin prospects, which then forms the basis of a reevaluation of the question whether lead, zinc and reduced sulphur could have been transported to the site of deposition by a single Na-Ca-K-Mg-Cl-CO_2 -rich brine. Thermodynamic mass transfer modelling based on the most recent experimental data on the solubility of galena and sphalerite suggests that formation of the deposit by a single fluid is possible, provided that the fluid originates from a clay-carbonate source region at temperatures > 150°C, and is rapidly focussed into a lower temperature deposition site. There, reaction of the acid fluid with calcite-rich rocks is predicted to result in carbonate dissolution, dolomitization and chloritization associated with base metal sulphide precipitation, in general agreement with geological observations.

Introduction

There have been numerous experimental studies on the solubility of lead and zinc in subcritical fluids (Nriagu, 1971a, 1971b, Barrett, 1974, Khodakovskiy and Yelkin, 1975, Seward, 1984, Ruaya and Seward, 1986 etc.). The most recent of these studies are by Bourcier and Barnes (1987) on the chloride and bisulphide complexes of zinc and by Barrett and Anderson (1988) on the chloro-complexes of lead and zinc. Anderson (1973, 1975) and McLimans (1977) used the available solubility data to determine the physico-chemical constraints on the transportation and deposition of lead and zinc sulphides in Mississippi Valley type (MVT) deposits. Sverjensky (1984) demonstrated the chemical basis of the possible link between the oil

field brines and the ore forming solutions in the MVT deposits and evaluated the possible role of fluid/rock interaction in the transportation and deposition of lead and zinc. Sverjensky (1986) has further reviewed various problems related to the genesis of MVT deposits.

The existing geochemical models for the genesis of the MVT deposits are either based on a single-fluid (metal and reduced sulphur or metal and oxidized sulphur transported in the same fluids; Sverjensky, 1986) or involve some mixing process between two different fluids. In particular, for deposits like Pine Point, where ore has been formed at relatively low temperatures (90-100°C compared to 175-220°C elsewhere), a two fluid and/or two source model is thought to be more realistic (Sverjensky, 1986). Such a model is supported by Kharaka et al. (1987) who have reported the existence of two distinct types of formation waters in the oil fields of central Mississippi Salt Dome Basin. Formation waters with high concentrations of lead and zinc have extremely low concentrations (< 0.02 mg/l) of H_2S while those enriched in H_2S (up to 85 mg/l) have very low lead-zinc values. More recently, Haynes et al. (1989) have proposed a single-fluid model with simultaneous transport of zinc and reduced sulphur in the fluids for the zinc deposits of Mascot-Jefferson City Zinc district.

In the present study calculations have been carried out to reevaluate, in light of the most recent experimental data, the possibility of generating economic concentrations of lead and zinc in relatively low temperature MVT deposits from fluids transporting both metals and reduced sulphur in the same solution. This is significant in understanding the genesis of a number of MVT deposits located in the Lennard Shelf of northern Canning Basin.

Characteristic Features of Lead-Zinc Deposits in the Lennard Shelf, North Canning Basin

The MVT deposits in the Lennard Shelf occurring mostly in the Paleozoic carbonate reefs have been studied in some detail. The characteristic features of these deposits are summarized as follows:

1. The MVT mineralization in the Lennard shelf (Cadjebut, Wagon-Pass, Narlarla etc.) are localized in partly dolomitized Devonian reef carbonates (Etminan et al., 1984; Murphy et al., 1986; Buchhorn, 1986, Ringrose, 1984).

2. The Blendevale deposit contains an estimated 20 mt (8.3% Zn, 2.5% Pb) of ores composed of marcasite, pyrite, sphalerite, galena and calcite occurring as veins and breccia cements formed during or after faulting of the host limestone.

3. In the Cadjebut deposit which contains 3 mt of ores (13.5% Zn and 4% Pb), mineralization is present in the form of stratabound and fracture filling sulphides in partly dolomitized Devonian carbonates .

4. In the Wagon-Pass and Narlarla deposits, mineralization occurs as disseminations, veinlets of sulphides in dolomitized and chloritized calcareous rocks. The sulphide mineralization at Wagon Pass seems to have postdated the main dolomitization and is related to brecciation and formation of late dolomite, calcite and chlorite.

5. At Blendevale, ore paragenesis includes an early stage of calcite, marcasite, sphalerite and galena followed by a second stage of barite and late calcite. Within the sulphide stage, sphalerite seems to have formed earlier than galena. At Wagon Pass the paragenesis is essentially the same with additional dolomite and chlorite in the early sulphide stage. Traces of chalcopyrite and bornite are also present.

6. The mineralization at Wagon-Pass and Narlarla and Cadjebut is associated with zones of pervasive chloritization and/or dolomitization of host rocks. Alteration zones up to a few hundreds of meters in thickness have been observed in the Wagon- Pass and Narlarla deposits (Ringrose, 1984). In contrast, the Blendedvale deposit is devoid of any significant alteration except some minor silicification of limestones.

7. C, O, and S-isotope data on the early cements in the unmineralized limestones indicate the presence of extensive marine cementation (Lambert and Etminan, 1987). In contrast, isotopic and limited fluid inclusion data from later cements (blocky calcite spars) indicate influx of hot (between 40 and 110°C) basinal brines.

8. Fluid inclusion studies in dolomite closely associated with mineralization indicate that brines at minimum temperatures of 70 to 110°C were involved in ore deposition (Etminan, 1986). Fluid inclusions in sphalerite from the Blendevale deposit show similar homogenization temperatures between 70 and 110°C. The absence of any signs of boiling indicates that the pressures were greater than the vapour pressure of the fluids and hence a pressure correction to the homogenization temperatures of about 10 to 80°C, assuming fluid pressures between lithostatic and hydrostatic pressures corresponding to a possible overburden of 1 to 3

kilometres. Last ice melting temperatures of inclusion fluids of -15 to -32°C indicate high salinity with appreciable amounts of calcium (laser mass spectrometry) and a K/Na ratio of 0.02 to 0.07 (leachate analysis)

8. Sulphur isotope analysis (Lambert, 1986) indicates that sulphate reduction was the main source of sulphur even though both thermochemical reduction (because of low temperatures and bacterial reduction (because of high temperatures of ore deposition) seem to be problematic for the observed intermediate temperature range.

9. The colour alteration in conodont fossils (Nicoll, pers. comm) and preservation of Pre-Devonian fission track ages in detrital apatites (Arne et al., 1988) indicate that the host rocks for the Pb-Zn deposits and permeable strata along which the metalliferous and dolomitizing fluids migrated were not heated above 70°C for substantial lengths of time.

Sources of Thermodynamic Data

Basic thermodynamic data on the stability of many aqueous species used in the following calculations has been obtained from the datafile SOLTHERM (Reed, 1982) which was modified by Heinrich (1987, file GIBBMRAQU, see Appendix)) to be compatible with the free energy data file CPDMRLDAT of the CSIRO-SGTE THERMODATA system (Turnbull and Wadsley, 1986) and with the free energies of aqueous ions tabulated by Cobble et al. (1982). The stability data on the chloro-complexes of lead and zinc have been obtained from Seward (1984) and Bourcier and Barnes (1987), respectively. Data for the bisulphide complexes of lead and zinc have been taken from Giordano and Barnes (1979) and Bourcier and Barnes (1987) respectively. Bourcier and Barnes (1987) have found close agreement ($\pm$ 0.3 log units) between their measured sphalerite solubilities and higher-temperature complexation constants measured by Ruaya and Seward (1986). Similarly, there is a good agreement with earlier extrapolations of low-temperature data by Helgeson (1969), at temperatures up to 350°C and salinities greater than 0.1m chloride. Data for aqueous chloride complexes of calcium ($CaCl^+$ and $CaCl_2$) have been obtained from Williams-Jones and Seward (1989). In the absence of basic stability data for $MgCl_2$(aq), the association constant of $CaCl_2$ (aq) was adopted to derive the free-energy data for $MgCl_2$(aq). Data for aqueous chloride complexes of iron ($FeCl^+$ and $FeCl_2$ were taken from Heinrich and Seward (1990).

Activity coefficients for the charged aqueous species were estimated using the extended Debye-Huckel equation of Helgeson (1969). The "distance of closest approach" parameter, å, for the chloro complexes of lead and zinc having stochiometries of M^{+2}, MCl^{+}, MCl_3^{-} and MCl_4^{-2} was taken as 5, 4, 4, and 5 respectively (Seward, 1984, Ruaya and Seward, 1986). For all bisulphide complexes of lead and zinc å was taken equal to 4.5 (Bourcier and Barnes, 1987). The å parameter for other charged aqueous species were taken from Truesdell and Jones (1974). An activity coefficients of one was adopted for all neutral aqueous species.

Thermodynamic data for most of the minerals were taken from the CPDMRLDAT file of Turnbull and Wadsley (1986). There is some difficulty in treating chlorite due to the complex nature of solid solution (Walshe,1986), and the thermodynamic properties of chlorite turn out to be one of the most important uncertainty in the modelling presented below. A fixed composition of chlorite $\{FeMg_4Al_2Si_3O_{10}(OH)_8\}$ has been assumed based on the available microprobe analysis of chlorites from the Canning Basin deposits. Basic thermodynamic data for chlorite of this composition has been derived by adding 1/5 plus 4/5 of the iron and magnesium end members, respectively, of Walshe (1986).

Speciation in the Pb-Cl-S-O-H and Zn-Cl-S-O-H Systems

Fig. 1 shows the predominance areas of aqueous lead and zinc species in fluids undersaturated in ZnS and PbS, with the activity of chloride equal to 2.5 and activities of sulphur species equal to $1x10^{-5}$ (Fig. 1a & b) and $1x10^{-2}$ (Fig. 1c & d).

In a high-salinity fluid (a_{Cl^-} =2.5), $ZnCl_3^-$ is the dominant complex under acidic conditions while in more alkaline conditions a bisulphide complex, Zn(OH)(HS) becomes dominant. With falling temperature the stability field of the chloro-complex narrows down and moves towards more acidic conditions (Fig. 1). Similarly for lead, chloro species ($PbCl_3^-$ and $PbCl_4^{-2}$) predominate under acidic conditions while in more alkaline conditions $Pb(HS)_2$ becomes dominant (Fig. 1c & d). Amongst the chloro species of lead, $PbCl_4^{-2}$ becomes stable only at temperatures below 125°C.

Fig. 2 shows contours of galena and sphalerite solubility in brines of the same chloride activity (2.5). The boundaries between the aqueous species and coexisting iron sulphides and oxides have been drawn at an

activity of dissolved iron species equal to $0.6x10^{-3}$. These calculations indicate that ZnS is considerably more soluble than PbS. Under f_{O2} values lower than the hematite/magnetite buffer the solubility is independent of the redox state and depends only on the pH, decreasing rapidly with increase in pH. Under higher f_{O2} conditions (where most of the sulphur is present as sulphate), the solubility of PbS and ZnS as chloro species becomes independent of pH and is determined mainly by the redox state of the system. Thus, as indicated earlier by Anderson (1973), in order to transport geologically realistic amounts of lead, zinc ($\geq$1ppm of each) and reduced sulphur in a single chloride fluid, the solutions must be very acidic (pH < 3 - 4 at 125°C and <4.5 and 5 at 200°C). The transportation of lead and zinc becomes more efficient under more oxidized conditions where most of the sulphur is present as sulphate. This however requires that the oxidation potential of the fluid must be at least 2 to 3 log units higher than the hematite/magnetite buffer. The presence of hydrocarbon-rich inclusions (Etminan and Hoffman, 1989) in the ore and gangue minerals indicate that at least at the time of ore deposition the redox conditions were lower than the hematite/magnetite buffer. Under reducing equilibrium conditions, significant sulphur and base metal co-transportation is therefore only possible at low solution pH. Relatively high activities of aqueous species of calcium (0.6) and magnesium (0.1) and dissolved CO_2 (0.6), in fluids buffered by carbonate rocks will favour high solution acidity (pH = 4 and less, see below). Depending on cation ratios and hence pH (but independent of oxidation potential) such an acid brine can transport up to 1-10 ppm of lead and zinc at temperatures as low as 150°C together with comparable concentrations (0.01m) of reduced sulphur (Fig. 2).

Fig. 2d indicates the effect of change in the activity of dissolved sulphur species on the solubility of PbS and ZnS. As expected the solubility of PbS and ZnS decreases appreciably with increase in the amount of total dissolved sulphur. Changes in the solubility of PbS and ZnS as a function of temperature and pH are shown in Fig. 3 At a fixed pH, the solubility of both PbS and ZnS falls rapidly with decreasing temperature. Also shown on the diagram are calcite (ca), dolomite (dol), muscovite - kaolinite (mc), and potash feldspar-quartz - muscovite (Kmq) buffers. A fluid cooled under rock buffered conditions (pH and redox controlled by the mineral assemblages of the wall rock) will start precipitating lead and zinc sulphides because of cooling as well as increase in the pH. In contrast, cooling under fluid buffered conditions (both pH and redox controlled by the fluid species) PbS

and ZnS precipitation may be inhibited because cooling of the fluid will be accompanied by a decrease in pH. Cooling in rock buffered and fluid buffered conditions will be investigated in more detail by using muticomponent mass-transfer calculations which are better suited to predict the overall effects of competing chemical reactions than activity diagrams. Equilibrium constants ($LogK_r$) of a number of reactions relevant to the present study are summarized in Table 1.

Mass-Transfer Calculations

In MVT deposits, most of the mineralization is localized in calcareous rocks (limestones and dolostones) which show evidence of dissolution of the carbonate host rock, including slumping, collapse breccias, or thinning of the host beds. In many deposits silicified, dolomitized and chloritized wall rocks envelop zones of mineralization, indicating that ore-forming fluids which migrated from the deeper parts of the sedimentary basin towards the site of deposition were out of chemical equilibrium with the unaltered calcite-rich wall rocks at the site of deposition.

The mass-transfer calculations undertaken in this study are aimed at evaluating the possibility of transporting geologically realistic amounts of lead, zinc and reduced sulphur in a fluid in equilibrium with the altered (chloritized and/or dolomitized) or impure limestones. Calculations have been performed for two model fluids (Table 2), the composition of which are based on analyses of oil field brines and fluid inclusions. The present-day hypersaline deep formation waters of the Canning basin are Na-Ca-Cl rich brines with salinities of up to 250,000 mg/l (Etminan et al., 1989; Ferguson and others, in prep.)) and are similar to oil-field brines from many other basins (Sverjensky, 1984, 1987, Kharaka et al., 1987). Fluid inclusion studies in ore and gangue minerals from various localities including lead-zinc prospects of Canning Basin have also revealed similar Na-Ca-Cl rich fluids of high salinity. Fluid inclusions from the zinc deposits of Mascot-Jefferson City Zinc district analyzed by Haynes et al. (1989) give the following individual ion molalities: Na (2.2-3.4m), Ca (0.3-0.8m), K (0.1-0.3m), and Mg (0.04-0.12m).

If the pH of the ore-forming fluids is buffered by the carbonate rocks, it will be controlled by the activities of CO_2 and relevant cations such as calcium and/or magnesium. Higher activities of calcium, magnesium and

dissolved CO_2 will generate more acidic conditions. Unfortunately there is little data on the concentration of CO_2 in the oil-field brines. The information on the CO_2 concentration in fluid inclusions is also limited. Haynes et al. (1989) have reported values of 0.4 to 1.5 mol% CO_2 based on gas-chromatographic analysis.

Solubility of PbS and ZnS as Function of Wall-Rock Mineralogy

The solubility of PbS and ZnS has been calculated for two model fluids in equilibrium with three different rocks: chloritized and dolomitized rock, siliceous dolostone and siliceous limestone (Table 3, Figs. 4 to 7). In all calculations an excess of rock is assumed i.e. a low fluid/ rock ratio of 1:10 and1:50 as one might expect to be realised in potential source regions of the ore fluids. Fluid A is used in combination with altered (chloritized and dolomitized) rock and siliceous dolostone to model the formation of Wagon-Pass, Narlarla and Cadjebut deposits where the mineralization is localized in altered rocks and siliceous dolostones. Fluid B is similar to Fluid A, except for lower concentration of magnesium. Fluid B is used in combination with siliceous limestone to model mineralization at the Blendevale deposit. Pyrite is present in chloritized and/or dolomitized rocks along with magnetite. In lead-zinc ores, pyrite and/or marcasite is an essential sulphide that was deposited paragenetically earlier than sphalerite and galena. Therefore in all calculations, lead-zinc carrying fluid is assumed to be saturated in pyrite controlling the activity of aqueous species of sulphur in the fluid.

Fig. 4 shows the solubility of PbS and ZnS in a fluid (fluid A, Table 2) buffered by an excess (Fluid/rock ratio of 1:50) of chloritized and dolomitized rock. The redox state of the fluid is buffered by the pyrite-magnetite assemblage while the pH is buffered by dolomite according to the following reactions:

$$3FeS_2 + 4H_2O + 2H_2\,(g) = Fe_3\,O_4 + 6H_2S\,(aq) \qquad (1)$$

$$CaMg(CO_3)_2 + 4H^+(aq) = Ca^{+2}(aq) + Mg^{+2}(aq) + 2CO_2(aq) + H_2O \qquad (2)$$

The solubility of ZnS decreases with temperature from 160 ppm at 150°C to 125 ppm at 100°C, whereas the solubility of PbS first increases from 35 ppm at 150°C to 49 ppm at 120°C and then falls to 40 ppm at 100°C

(Fig. 6a). Under these conditions, the dominant species of lead and zinc in the fluid are $PbCl_3^-$, $PbCl_4^{-2}$ and $ZnCl_3^-$, $ZnCl_4^{-2}$ respectively.

A similar fluid with 100 times lower concentration of dissolved CO_2 (0.06m instead of 0.6m) under similar rock buffered conditions can dissolve 10 to 20 times less ZnS and PbS because of its lower acidity (Fig. 5). The solubility of PbS and ZnS increases slightly with falling temperature, from 7 and 1.6 ppm of zinc and lead, respectively, at 150°C, to 12 and 4 ppm at 100°C (Fig. 5).

A saline, CO_2-rich fluid (Fluid A, Table 2, CO_2 = 0.6m) buffered by a siliceous dolostone is able to dissolve 3 to 4 times less lead and zinc (compare Figs. 4 and 6). The solubility of PbS and ZnS decreases with falling temperature, from 53 and 11 ppm ppm of zinc and lead at 150°C, to 9 and 3 ppm at 100°C. Under these conditions the dominant species of lead and zinc in the fluid are $PbCl_3^-$, $PbCl_4^{-2}$ and $ZnCl_3^-$, $ZnCl_4^{-2}$ respectively. Throuhghout the following calculations, the redox state of the fluid is kept in the stability field of reduced sulphur, controlled by the CO_2/CH_4 pair according to the following reaction:

$$CO_2\,(g) + 3H_2\,(g) = CH_4\,(g) + 2H_2O \qquad (3)$$

The pH of the fluid is buffered by dolomite (reactions 2).

When a CO_2-rich fluid (fluid B, Table 2) is buffered by a siliceous limestone it can dissolve up to 4 to 5 times less lead and zinc (compare Figs. 4 and 7). In such a fluid the solubility of ZnS and PbS falls from 40 and 8 ppm zinc and lead respectively at 150°C to 8 and 3 ppm at 100°C (Fig. 7). Under these conditions the dominant species of lead and zinc in the fluid are $PbCl_3^-$, $PbCl_4^{-2}$ and $ZnCl_3^-$, $ZnCl_4^{-2}$ respectively. The pH is buffered by calcite according to the reaction:

$$CaCO_3 + 2H^+(aq) = Ca^{+2}(aq) + CO_2(aq) + H_2O \qquad (4)$$

In summary, the calculations on the solubility of galena and sphalerite indicate that acid fluids with sufficiently high concentrations of calcium, magnesium and CO_2, buffered by carbonates and saturated with respect to pyrite, are capable of transporting realistic concentrations of lead and zinc from a potential source region at 100-200°C through a sequence of impure limestones and dolostones.

Cooling of Fluids Under Rock-Buffered Conditions

The solubilities of PbS and ZnS under rock-dominated (low fluid/rock) conditions discussed above form the basis of evaluating the behaviour of lead and zinc in a fluids which undergoes cooling under rock-dominated (low fluid/rock ratio) conditions.

A fluid saturated in PbS and ZnS at 150°C, when cooled in the presence of chloritized and dolomitized rock (cf. Fig. 8) becomes undersaturated in PbS due to increase in its solubility with fall in temperature (Fig. 4). ZnS begins to precipitate at 150°C but dissolves immediately and starts reprecipitating below 130°C. On reaching 100°C, up to 25% of the total dissolved zinc precipitates as ZnS. An undersaturated fluid, when cooled under similar rock buffered conditions will remain undersaturated in PbS and ZnS and will not deposit PbS or ZnS.

The behaviour of PbS and ZnS during cooling of saturated and undersaturated fluids buffered by the siliceous dolostone and limestone is different from that described above. A fluid saturated at 150°C when cooled in the presence of an excess of siliceous dolostone (1kg of fluid with 50 kg of rock) starts precipitating ZnS and PbS at 150°C and on reaching 100°C, 84% of its initial Zn and 75% of it's initial lead are precipitated as ZnS and PbS respectively (Fig. 9). The fluid is saturated with respect to pyrite at 150°C but on cooling becomes increasingly undersaturated, leading to its dissolution. An undersaturated fluid precipitates PbS and ZnS at lower temperatures. Fig. 10 shows cooling of a fluid, undersaturated in lead and zinc by 50%. The precipitation of ZnS begins at 130°C followed by PbS at 120°C.

A fluid saturated in PbS and ZnS at 150°C when cooled in the presence of an excess of siliceous limestone (fluid/rock ratio of 1:10) starts precipitating PbS and ZnS at 150°C and on reaching 100°C, 80% of it's initial zinc and 70% of it's lead are deposited as ZnS and PbS (Fig. 11). On cooling the fluid gradually becomes undersaturated in calcite and pyrite which leads to dissolution of these minerals. This is accompanied by simultaneous precipitation of quartz and dissolution of pyrite. An undersaturated fluid starts precipitating ZnS and PbS at 120°C (Fig. 12).

These calculations have shown that cooling of saturated and undersaturated fluid under rock buffered can lead to deposition galena and sphalerite from fluids moving through siliceous dolostones and limestones.

In both the cases a drop in the solubility with falling temperature is the dominant factor that controls mineral deposition.

Single-Step Fluid-Rock Reaction

A saturated fluid cooled in equilibrium with chloritized and dolomitized rock will only precipitate sphalerite (Fig. 8) because the solubility of PbS under such conditions increases with falling temperature and the solution becomes progressively undersaturated with respect to galena. One possible way of precipitating galena from such a fluid is by reacting this fluid with an unaltered limestone at some lower temperature, which will drive base metal saturation due to an increase in solution pH.

Fig. 13 represents such a fluid-rock reaction in which a fluid, initially undersaturated with respect to PbS and ZnS, reacts with calcite under low fluid rock ratio of 1:10, at variable temperature plotted on the horizontal axis. This fluid, which was initially buffered by dolomitized and chloritized rock at 150°C, reacts with limestone, partially dolomitizing it. With the appearance of dolomite, the solution pH becomes buffered by the calcite-dolomite assemblage by the following equilibrium:

$$CaMg(CO_3)_2 + 2H^+(aq) = CaCO_3 + Mg^{+2}(aq) + CO_2(g) + H_2O \qquad (5)$$

The redox state of the fluid is controlled by the CO_2/CH_4 pair. The intensity of dolomitization is higher at higher temperatures. At 130°C and above, fluid remains undersaturated with respect to PbS and ZnS and the precipitation of these minerals occurs at temperatures below 130°C. Dolomitization of limestone is accompanied by the deposition of quartz. This reaction does not form chlorite at any temperature, while pyrite precipitates only at temperatures above 100°C. Higher amounts of fluid (fluid/rock ratio of say 50 and above) will be able to completely dolomitize the rock, leading to proportionately higher base metal concentrations in the final rock. This simple computational model for fluid-rock reaction represents a physical process, in which a large batch of fluid initially buffered by dolomitized and chloritized rock would be focussed into a relatively small amount of unaltered limestone at lower temperature and equilibrates with it in a single step. Considering the relatively small porosity (i.e. *instantaneous* fluid/rock

ratio) even of a brecciated rock, this model does not afford a geologically very realistic description of hydrothermal alteration by fluid advection.

Progressive Fluid-Rock Interaction

Figs. 14 to 18 shows the results of a model for fluid-rock interaction that may be geologically more realistic. In this case a large quantity of a fluid (10 kg) initially buffered by altered rock (chloritized and dolomitized wall rocks lining the aquifer) reacts with with a small amount (0.1 kg) of fresh siliceous limestone in a series of smaller batches, each batch (0.1 kg) reacting successively with the limestone and thereby altering it in a progressive manner. Integrated fluid/rock ratio, marked along the horizontal axes of Figs 14 to 18, is given by the number of batches of fluid (i.e quantity of fluid) that have reacted with the same fixed quantity of siliceous limestone. Increasing integrated fluid/rock ratio therefore represents increasing intensity of alteration of the rock.

At depositional temperatures between 140 and 100°C, limestone is successively replaced by dolomite with increasing the fluid/rock ratio, and at a fluid/rock ratio > 60 calcite is completely consumed. During dolomitization of the siliceous limestone, pH is buffered by the dolomite-calcite assemblage (reaction 5) while the redox potential is controlled by the CO_2/CH_4 pair (reaction 3). At fluid/rock ratio >70, with the appearance of chlorite, magnetite and pyrite and the disappearance of calcite the pH and redox buffering shifts abruptly due to the change to dolomite and magnetite-pyrite assemblage (see reactions 1 & 2). The degree of saturation with respect to PbS and ZnS also changes with increasing intensity of reaction. At 140°C and130°C (Figs. 14 & 15) sphalerite starts redissolving at high fluid/rock ratios (> 70) after the disappearance of calcite and deposition of chlorite and pyrite. At 140°C, the fluid becomes undersaturated in sphalerite and all the earlier precipitated sphalerite dissolves completely (Fig. 15). At 120°C and below the fluid remains saturated with respect to sphalerite and deposits sphalerite continuously throughout the reaction.

With respect to galena the fluid remains undersaturated at 120°C and above. At 120°C the fluid initially deposits galena at low fluid/rock ratios but with the increase in the intensity of reaction, galena dissolves completely (Fig. 16). At lower temperatures the dissolution of galena is very minor and bulk of the precipitated galena is retained in the rock (Figs. 17 & 18).

These calculations indicate that a fluid initially buffered by a chlorite-dolomite rock at high temperature will at lower temperature react with a fresh siliceous limestone and progressively transform it into a rock containing secondary chlorite and dolomite. During this process, sphalerite and galena precipitated in the early part of the reaction (low fluid/rock ratio) will dissolve completely with increasing intensity of reaction. In this process sphalerite will be retained at 130°C and below while galena will be deposited at 110°C and below. For a dynamic system where fluids flow from a relatively hot source region towards a cooler depositional environment, the modelling predicts that sphalerite and galena, first deposited at relatively high temperatures, will later be dissolved and reprecipitated at lower temperatures. This will lead to a gradual accumulation of base metal sulphides and progressively increasing ore accumulation at an alteration front that advances down the temperature gradient and in the direction of fluid flow. The calculations would also predict a base metal zonation, in this case with sphalerite enrichment (relative to galena) near the higher-temperature, 'upstream' end of the alteration system. Conversely, if simple fluid cooling was the dominant mineralizing mechanism, an inverse zonation with galena near the higher-temperature end of the system might be expected.

The process of advancing dolomitization is also predicted to occur in chlorite-free limestone, again associated with progressive dissolution and reprecipitation of sphalerite and galena. This could apply to the formation of the Cadjebut deposit, which is localized in dolomitized limestones without chlorite. Fig. 19 represents such a reaction in which 10 kg of a fluid initially buffered by a dolomitized rock reacts progressively with 0.1 kg of a siliceous limestone at 130°C. With the increasing fluid-rock interaction, the dolomitization of limestone intensifies. During dolomitization, when calcite and dolomite coexist, pH of the fluid is buffered by the calcite-dolomite reaction. After the complete removal of calcite from the rock, pH drops and the buffering shifts back to dolomite. The fluid remains saturated with respect to ZnS and deposits sphalerite throughout the reaction. With respect to PbS, the fluid is saturated at the low fluid/rock ratios but becomes undersaturated at the fluid/rock ratio >70 and starts dissolving it.

Summary of Modelling Results

The chemical modelling described in the earlier sections indicates the following results:

a) At 150°C and below, near-neutral chloride-rich fluids, buffered with regard to acidity by the mica-clay (mc) or K-feldspar-mica-quartz assemblages, cannot transport significant concentrations of reduced sulphur and base metals (1ppm) together under equilibrium conditions (Fig. 2). Oxidized fluids containing most of their sulphur in the form of sulphate can transport much larger amounts of lead and zinc, depending on redox potential which controls the ratio of oxidized to reduced sulphur.

b) In fluids buffered by rocks rich in carbonates ± clays ± quartz (but without mica/feldspar in equilibrium with the fluid), potentially lower pH conditions permit co-transportation of significant concentrations of reduced sulphur and base metals. For example, a chloride-rich fluid with high but realistic concentrations of calcium (0.6m), magnesium (0.1m) and dissolved CO_2 (0.6m), when buffered by a pyrite-chlorite-dolomite rock, can dissolve up to 160 ppm zinc and 125 ppm lead at 150°C. The concentration of H_2S will be significant but probably lower, controlled by the relative stability of pyrite and Fe-chlorite (which is thermodynamically not very well characterized). The solubility of sphalerite in such a fluid decreases slightly with decreasing temperature, to 125 ppm zinc at 100°C, while the solubility of galena increases slightly to 40 ppm zinc at 100°C. Base metal solubilities strongly depend on pH, which in turn is controlled by the activity of calcium, magnesium and CO_2 through carbonate buffer equilibria (2,4). A fluid with 100 times lower concentration of CO_2 (0.06 instead of 0.6m) is able to carry 20 times less lead and zinc. When the fluids are buffered by the chloritized and dolomitized rock, their pH is controlled by dolomite, while the redox state is buffered by the magnetite-pyrite assemblage (reactions 1&2).

c) Chloride-rich fluids, buffered by siliceous dolostone and limestone, are able to dissolve 3 to 4 times less galena and sphalerite. The solubility of galena and sphalerite falls with decreasing temperatures. For such fluids, pH is buffered by dolomite and calcite respectively while the redox state is controlled by the CO_2/CH_4 pair.

d) Cooling of fluids, initially saturated or undersaturated in lead and zinc at 150°C, in equilibrium with an excess of the chloritized and dolomitized rocks keeps the fluids undersaturated with respect to galena, while the precipitation of sphalerite commences below 130°C.

e) Cooling a saturated fluids below 150°C in equilibrium with an excess of siliceous dolostone or siliceous limestone leads to the precipitation of galena and sphalerite immediately below 150°C. When the fluids are undersaturated in lead and zinc the precipitation begins at lower temperatures. Sphalerite precipitates first, followed by galena at even lower temperature.

f) Reaction of a brine that is initially buffered by chloritized and dolomitized rock and saturated in lead and zinc at 150°C, with siliceous limestone results in dolomitization and chloritization. At low fluid/rock ratios, i.e. at lower degree of fluid-rock interaction, the fluid precipitates sphalerite which at 140°C and above may redissolve completely after exhaustive replacement of calcite by dolomite and the appearance of chlorite, magnetite and quartz as stable minerals in the altered rock. At 130°C and below the fluid remains saturated with respect to sphalerite and deposits sphalerite throughout the reaction. With respect to galena, the fluids remain undersaturated at 120°C and higher temperature. Below 120°C the fluids are saturated with respect to galena and deposit galena. Model calculations of progressive, open-system fluid-rock interaction indicate that a fluid, buffered by dolomitized and chloritized rocks along a flow path from higher to lower temperatures, is likely to cause progressive alteration of limestone. During this process sphalerite and galena precipitated earlier at relatively higher temperatures are dissolved and reprecipitated at lower temperatures, thereby contributing to a progressive enrichment of base metal ore grades.

g) For fluids buffered by siliceous limestone or siliceous dolostone, rock -buffered cooling of the fluidcan be an effective mechanism of galena and spaherite deposition. If the fluid is buffered by the chloritized and dolomitized rock containing pyrite and magnetite, rock-buffered cooling will deposit sphalerite only. In order to deposit galena as well, progressive reaction of this fluid with siliceous limestone is predicted as the most efficient mechanism of mineralization.

Conclusions

In most of the known MVT deposits of the Canning Basin, ore is hosted by siliceous limestones that were dolomitized and/or chloritized during the mineralization process. The deposition of base metal sulphides is associated with net dissolution of carbonates as indicated by high

porosity/permeability of mineralized breccias. The altered rocks contain paragenetically early pyrite or marcasite as common ore mineral, but it is not entirely clear whether this iron sulphide was emplaced by a separate process preceding lead-zinc mineralization, or whether they formed as an outer halo at the time of base metal deposition. Irrespective of this, the Na-Ca-Mg-Cl brines carrying lead, zinc and reduced sulphur, may be assumed to be in chemical equilibrium with the altered rocks (dolomite + quartz + pyrite ± calcite ± chlorite) at the deposition site and probably along parts of their flow path from hotter parts of the basin.

Chemical modelling based on this assumption and a variety of likely wall rock mineral assemblages suggests that high concentrations (10-100 ppm) of lead and zinc could be transported in a single chloride brine at temperatures below 150°C, provided that the solution is sufficiently acid. This is possible provided that Na-K-Ca-Mg-Cl-CO_2 brines with high CO_2 and earth alkali concentrations originated from a relatively hot source region (temperatures in excess of about 150°C) in which carbonates, clays and/or chlorite were saturating minerals, but in which feldspars were absent or out of chemical equilibrium with the fluid. Sphalerite and galena may be precipitated from such a fluid either by simple cooling or, more efficently, by reaction with calcite-rich carbonate rocks at lower temperature. Mass transfer calculations predict that the latter process is associated with net carbonate dissolution, replacement of calcite by dolomite, and precipitation of chlorite. Although not disproving a fluid mixing mechanism, these predictions agree with the widespread presence of collapse breccias, dolomitization of limestone, and chloritization observed in many MVT deposits in the Canning Basin and elsewhere. The most efficient mineralization process is predicted to result from rapid fluid flow from a hotter source region in to a cooler depositional site, which is consistent with the indications from the Canning Basin that the ore deposits represented transient thermal anomalies (mineralization temperatures between 80 and 90°C but generally > 100°C) compared with regional background temperatures (< 70°C indicated by conodont alteration and fission track data). Lead : zinc ratios in the final ores depend not only on the concentration of metals in solution and their availability in the fluid source region, but are also strongly affected by different extraction efficiency, to the extreme that under some conditions only one of the sulphides may precipitate from a fluid containing similar concentrations of both metals.

The most significant uncertainty in the preliminary chemical modelling presented here concerns the role of pyrite/marcasite in the paragenesis of the deposits, and the thermochemistry of chlorite (which is not well constrained by experimental data). The available data suggests that mass balance constraints and equilibria involving these iron compounds exert the dominant control on a fluid's ability to transport reduced sulphur, and this in turn controls the efficiency of potential mechanisms of galena and sphalerite accumulation by a single ore fluid.

Further work is in progress to test and improve the thermodynamic data base, by comparing predicted fluid compositions with published data from well-studied active geothermal and basin brine systems. In addition, further geological information about the relative abundance (even rough estimates) and spatial distribution of galena, sphalerite, secondary dolomite and, in particular, the iron minerals chlorite, magnetite and pyrite/markasite will be essential for testing and refining the quantitative chemical models for ore deposition.

References

Anderson, G. M., 1973, The hydrothermal transport and deposition of galena and sphalerite near 100°C: Econ. Geol., v. 68, p. 480-192.

Anderson, G., M., 1975, Precipitation of Mississippi valley type ores: Econ. Geol., v. 70, p. 937-942.

Arne, D. C., Green, P. F., Duddy, I. R., Gleadow A. J. W., Lovering, J. F., and Lambert, I. B., 1988, An apatite fission track study of Zn-Pb mineralization on the Lennard shelf, W. Australian Geol. Soc. Australia, abstract No. 21, 9th Australian Geological Convention, Feb. 1-5 1988, p. 50.

Barnes, H., L., 1979, Solubilities of ore minerals: in Barnes, H., L., (ed.) Geochemistry of hydrothermal ore deposits, New York, Wiley Intersci., p. 404-460.

Barrett, T. J., 1974, Solubility of galena and sphalerite in sodium chloride brines up to 95°C: Unpub. M.Sc. thesis, Univ. Toronto, pp.157

Barrett, T. J., and Anderson, G. M., 1988, The solubility of sphalerite and galena in 1-5m NaCl solution to 300°C: Geochim. Cosmochim Acta., v. 52, p. 813-820.

Bourcier, W. L., and Barnes, H. L., 1987, Ore solution chemistry- VII. Stabilities of chloride and sulphide complexes of zinc to 350°C: Econ. Geol., v. 82, p. 1839-1863.

Buchhorn, I. J., 1986, Geology and mineralization of the Wagon Pass prospect, Napier Range, Lennard Shelf, W. Australia: in Proceedings 13th Congress of the Council of Mining and Metallurgical Institution, v. 2, p. 163-172.

Cobble, J. W., Murray, R. C., Turner, P. J., and Chen, K., 1982, High temperature thermodynamic data for species in aqueous solutions: Nat. Tech. Inform. Service Report. EPRI-NP-2400, pp. 197.

Etminan H., 1986, Origin of lead-zinc deposits, Canning Basin, W. A., part II: Fluid Inclusion studies, Extended abstract, B. M. R. Symposium, p. 5-8.

Etminan, H., 1989, Present day formation waters provide clues to origins of Canning Basin Zn-Pb deposits: BMR Research Newsletter, no. 11, p. 6-8.

Etminan, H., and Hoffmann, C., 1989, Biomarkers in fluid inclusions: A new tool in constraining source regimes and its implications for the genesis of Mississippi Valley Type deposits: Geology, v. 17, p. 19-22.

Etminan. H., Lambert. I. J., Buchhorn. I. J., Chaku. S., and Murphy. G. C.,1984, research into diagenetic and mineralising processes, Lennard Shelf reef complex, W. A., in, Purcell. P. G., et al., ed., Proceedings of Geol Soc. Aust/Pet. Exp. Soc. Aust. Symposium, Perth, p. 447-454.

Giordano, T. H., and Barnes, H. L., 1979, Ore solution chemistry. VI. PbS solubility in bisulphide solutions to 300°C: Econ. Geol., v. 74, p.1637-1646.

Haynes, F. M., Beane, R. E., and Kesler, S., 1989, Simultaneous transport of metal and reduced sulphur, Mascot-Jefferson City Zinc district, East Tennessee: evidence from fluid inclusions: Am. J. Sci., v. 289, p. 994-1038.

Heinrich, C.A., 1987, The CSIRO-SGTE-THERMODATA package for thermodynamic computations at BMR. BMR Record 1987/42, 42pp.

Heinrich, C. A., and Seward, T. M., 1990, A spectrophotometeric study of aqueous iron(II) chloride complexation at 25 to 200°C: for Geochim. et. Cosmochim. Acta, in press

Kharaka, Y. K., Maest. A. S., Carothers, W. W., Law. L. M., Lamothe, P. J., and Fries, T. L., 1987, Geochemistry of metal rich brine from central Mississippi salt dome basin: Applied Geochemistry, v. 2, p. 543-561.

Khodokovsky, I. L., and Yelkin, A. E., 1975, Experimental determination of zincite solubility in water and aqueous NaOH solutions at temperatures of 100, 150, and 200°C: Geokhimiya, no.10, p. 1490-1495.

Lambert, I. B., 1986, Origins of lead-zinc deposits, Canning Basin, W. A., part I: Isotopic and related studies, Extended abstract, B. M. R. Symposium, p. 5-8.

Mclimans, R. K., 1977, Geological, fluid inclusion, and stable isotope studies of the upper Mississippi valley zinc-lead district, south west Wisconsin: Unpubl. Ph.D thesis, Pennsylvania State University, pp. 175.

Murphy. G. C., Bailey, A., Parrington. P. C., 1986, The Blendevale carbonate-hosted zinc/lead deposit, Pilara, Kimberley region, Western Australia., in Proceedings 13th Congress of the Council of Mining and Metallurgical Institutions, v. 2, p. 153-161.

Nriagu, J. O., 1971a, Studies in the system PbS-NaCl-H_2S-H_2O: Stability of lead(11) thiocomplexes at 90°C: Chem. Geol., v. 8, p. 229-310.

Nriagu, J. O., 1971b, Experimental investigations of a portion of the system PbS-NaCl-HCl-H_2O at elevated temperatures: Am. J. Sci., v. 271, p. 157-169.

Reed, M. H., 1982, Calculation of multicomponent chemical equilibria and reaction processes in systems involving minerals, gases and an aqueous phase: Geochim. Cosmochim. Acta., v. 46, p. 513-528 [Introduction to SOLTHERM data file].

Ringrose, C., R., 1984, The geology and genesis of the lead-zinc deposits, Napier Range, W. Australia: in Pincell et al. (eds.) Proceedings Of Geol. Soc. Aust/Pet. Exp. Soc. Aust. Symposium,Perth, p. 455-462.

Ruaya, J. R., and Seward, T. M., 1986, The stability of chlorozinc(II) complexes in hydrothermal solutions up to 350°C: Geochim. Cosmochim. Acta., v. 50, p. 651-661.

Seward, T. M., 1984, The formation of lead(II) chloride complexes to 300°C: a spectrophotometric study: Geochim.Cosmochim. Acta., v. 48, p. 121-134.

Sverjensky, D. A., 1984, Oil field brines as oreforming solutions: Econ. Geol., v. 79, p. 23-37.

Sverjensky. D. M., 1986, Genesis of Mississippi valley-type lead-zinc deposits: Ann. Rev. Earth Planet. Sci., v.14, p. 177-199.

Sverjensky. D. M., 1987, The role of migrating oilfields brines in the formation of sediment-hosted Cu-rich deposits: Econ. Geol., v. 82, p. 1130-1141.

Turnbull. A. G., and Wadsley M. W., 1986 The CSIRO-SGTE THERMODATA system. Introduction; Databank index; FILER; ESTIMA; REACT; SYSTEM; CHEMIX; VAPOUR; ENERGY; 9 vols., CSIRO Div. Mineral Chemistry., Port Melbourne.

Truesdell. A. H., and Jones. B. F., 1974, WATEQ, a computer program for calculating chemical equilibria of natural waters: Jour. Research U.S.Geol. Survey., v. 2, p. 233-246.

Walshe, J. L., 1986, A six-component chlorite solidsolution model and the conditions of chlorite formation in hydrthermal and geothermal systems: Econ. Geol., v. 81, p. 681-703.

Williams-Jones. A. E., and Seward. T. M., 1989, The stability of calcium chloro-complexes in aqueous solutions at temperatures between 100°C and 360°C: Geochim. Cosmochim. Acta, v. 53, p. 313-318.

Table 1

Equilibrium Constant for some Important Reactions

Reaction	$\log K_r$ (Temperature in deg C)					
	100	110	120	130	140	150
$CaCO_3 + 2H^+ = Ca^{+2} + CO_2(aq) + H_2O$	7.104	7.142	7.157	7.149	7.122	7.076
$CaMg(CO_3)_2 + 4H^+ = Ca^{+2} + Mg^{+2} + 2CO_2(aq) + H_2O$	13.19	13.09	12.98	12.85	12.72	12.57
$CaMg(CO_3)_2 + 2H^+ = CaCO_3 + Mg^{+2} + CO_2(aq) + H_2O$	6.091	5.952	5.823	5.705	5.596	5.495
$CO_2(g) + 4H_2(g) = CH_4(g) + H_2O$	14.03	13.11	12.24	11.42	10.64	9.899
$3FeS_2 + 4H_2O + 2H_2(g) = Fe_3O_4 + 6H_2S(aq)$	-31.9	-30.6	-29.3	-28.1	-26.9	-25.8
$PbS + 3Cl^-(aq) + 2H^+(aq) = PbCl_3^-(aq) + H_2S(aq)$	-3.48	-3.13	-2.77	-2.42	-2.08	-1.73
$ZnS + 3Cl^-(aq) + 2H^+(aq) = ZnCl_3^-(aq) + H_2S(aq)$	-2.02	-1.68	-1.33	-0.96	-0.60	-0.22

Table 2

Composition* of Hypothetical Ore Forming Fluids used in the Calculations
(concentrations in moles/kg water)

Component	Fluid A	Fluid B
NaCl	2.2	2.2
KCl	0.07	0.07
$CaCl_2$	0.6	0.7
$MgCl_2$	0.1	0.01
$FeCl_2$	0.006	0.006
SiO_2 (aq)	0.35	0.35
H_2S	$1x10^{-4}$-$1x10^{-6}$	$1x10^{-6}$
CO_2	0.06-0.6	0.6
CH_4	-	$0.12x10^{-6}$

* compositions are based on the analyses of oil-field brines and fluid inclusions (Etminan, Ferguson and others, unpublished data; Sverjensky, 1984; Haynes et al., 1989)

Table 3

Modal Mineral Composition of Hypothetical Rocks used in the Calculations

a) Chloritized and Dolomitized Rock

Mineral		mole/kg rock	vol%
Quartz	SiO_2	2.5	15
Chlorite	$FeMg_4Al_2Si_3O_{10}(OH)_8$	0.51	30
Dolomite	$CaMg(CO_3)_2$	2.94	54
Magnetite	Fe_3O_4	0.04	0.8
Pyrite	FeS_2	0.02	0.2

b) Siliceous Limestone

Quartz	SiO_2	0.63	3.8
Calcite	$CaCO_3$	9.6	96.
Pyrite	FeS_2	0.02	0.2

C) Siliceous Dolostone

Quartz	SiO_2	0.63	3.8
Dolomite	$CaMg(CO_3)_2$	5.2	96.
Pyrite	FeS_2	0.02	0.2

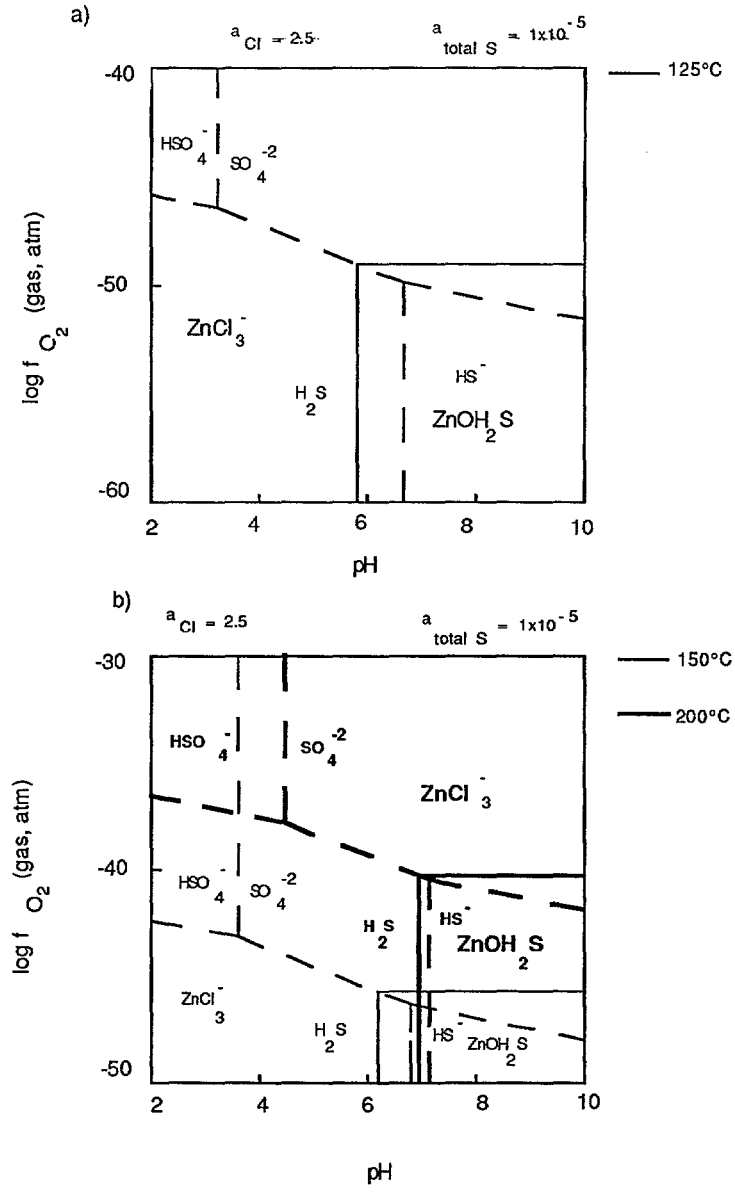
a)
$a_{Cl} = 2.5$
$a_{total\ S} = 1x10^{-5}$
125°C
-40
-50
-60
HSO_4^-
SO_4^{-2}
$ZnCl_3^-$
H_2S
HS^-
$ZnOH_2S$
2
4
6
8
10
pH
log f O_2 (gas, atm)
b)
$a_{Cl} = 2.5$
$a_{total\ S} = 1x10^{-5}$
150°C
200°C
-30
-40
-50
HSO_4^-
SO_4^{-2}
$ZnCl_3^-$
H_2S
HS^-
$ZnOH_2S$
2
4
6
8
10
pH
log f O_2 (gas, atm)

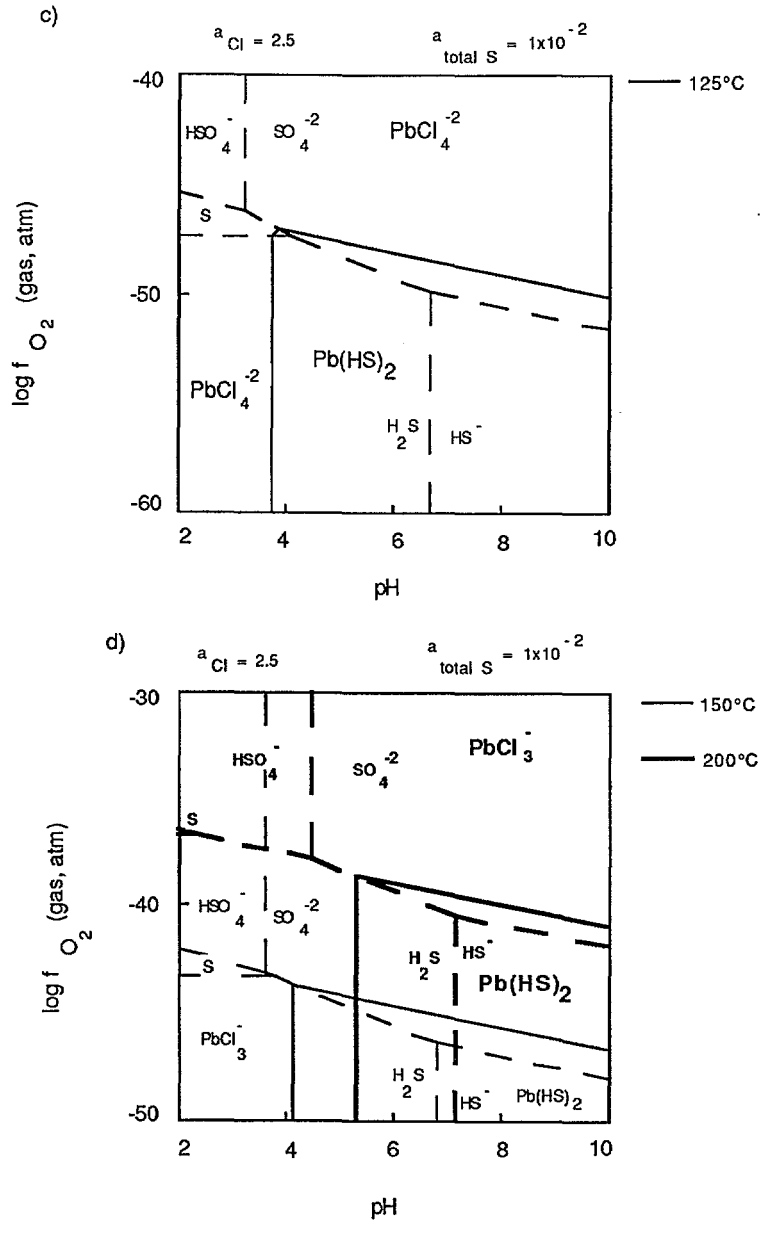

Fig 1. log fO_2 - pH diagram showing the stability fields of aqueous species of zinc (1a & b) and lead (1c & d). Dashed lines indicate the stability fields of aqueous species of sulfur.

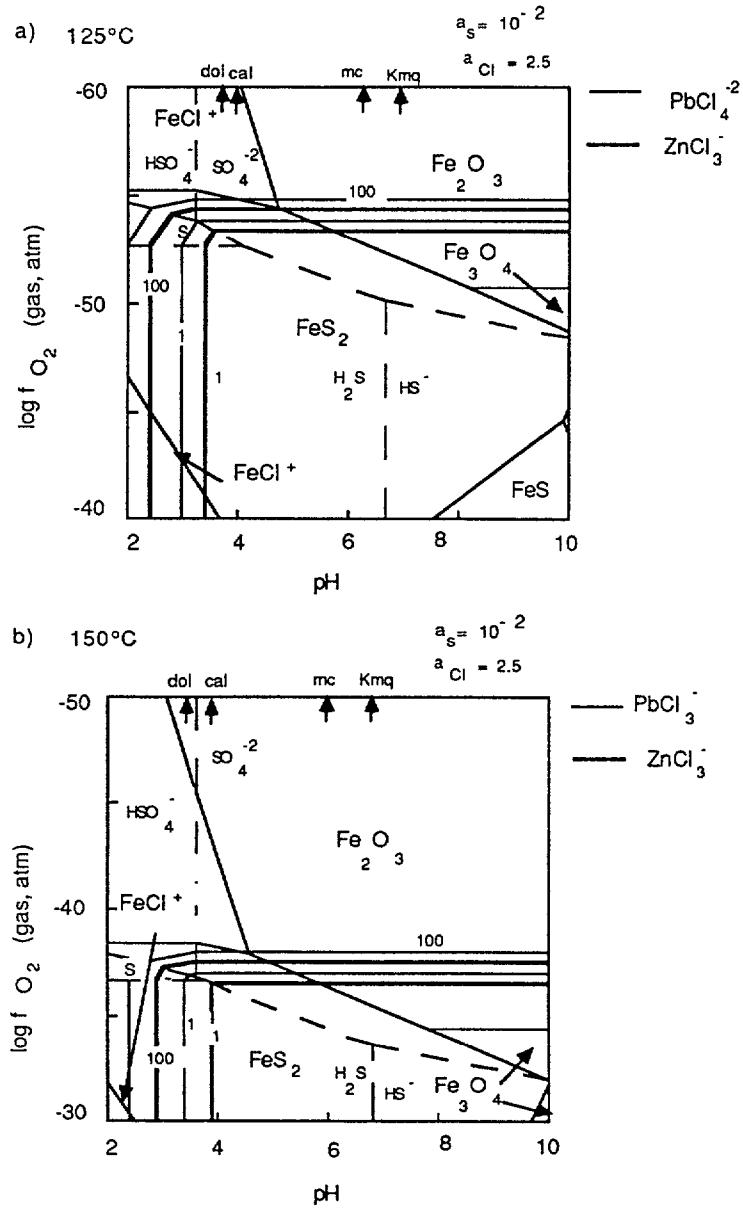
a) 125°C
$a_S = 10^{-2}$
$a_{Cl} = 2.5$
dol cal
mc Kmq
$PbCl_4^{-2}$
$ZnCl_3^-$
$FeCl^+$
HSO_4^-
SO_4^{-2}
Fe_2O_3
100
S
Fe_3O_4
FeS_2
H_2S
HS^-
FeS
log f O_2 (gas, atm)
pH
b) 150°C
$a_S = 10^{-2}$
$a_{Cl} = 2.5$
$PbCl_3^-$
$ZnCl_3^-$

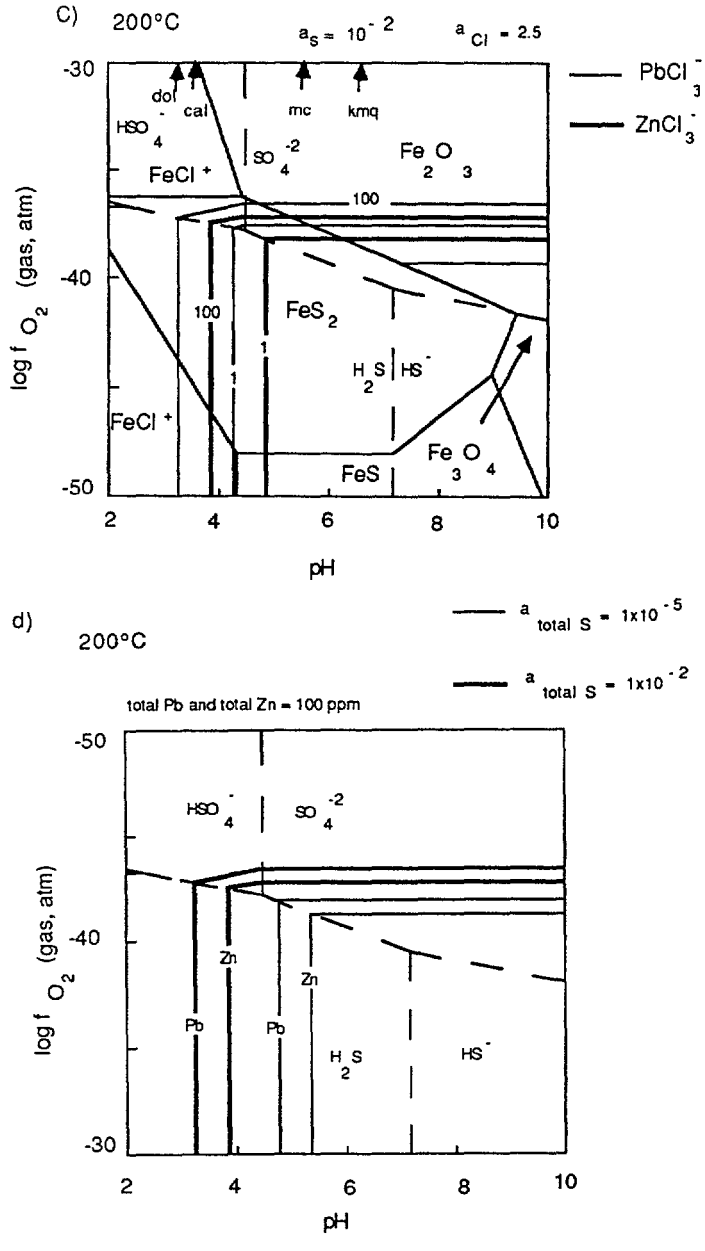

Fig 2. log f_{O2} - pH diagram showing the solubility of PbS and ZnS in the form of solubility contours in ppm (lines marked with numbers). Dashed lines indicate the stability fields of the aqueous species of sulfur for a $_S = 10^{-2}$. Also shown are the stability fields of iron oxides and sulfides. The boundary between $FeCl^+$ (aq) and pyrite has been drawn for a $_{FeCl^+} = 0.6x10^{-3}$. Short arrows on the upper pH-axis indicate the position of important pH-buffers: dol - dolomite buffer (eqn. 5), cal - calcite buffer (eqn. 4) , mc - muscovite+ kaolinite buffer, kmq- potash-feldspar+muscovite+quartz buffer. a) at 125°C, b) at 150°C , c) at 200°C, d) solublity of PbS and ZnS as a function of the activity of dissolved sulfur at 200°C. lead and zinc are present as $PbCl_3^-$(aq) and $ZnCl_3^-$(aq) respectively.

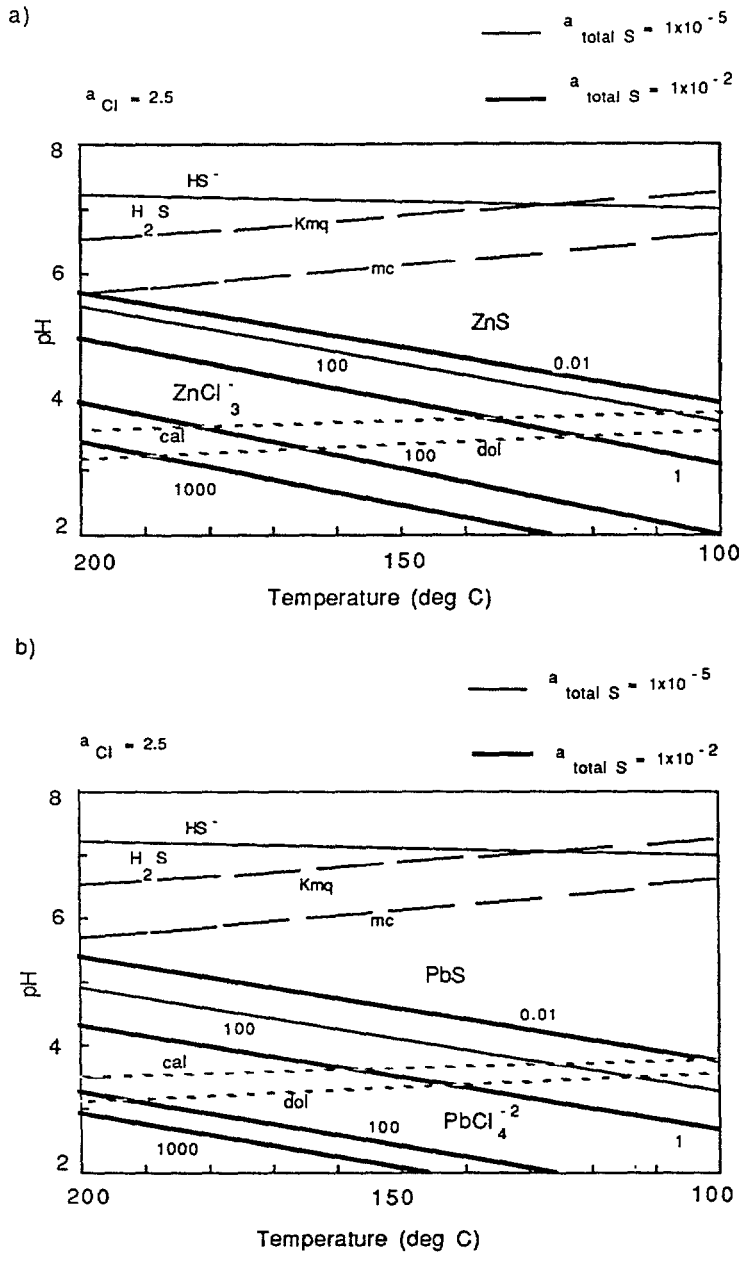

Fig 3. pH - T diagram showing solubility of PbS and ZnS (in ppm) in a saline fluid. Also shown is the boundary between aqueous H_2S and HS^-. Wide spaced dashed lines marked mc and kmq represent the muscovite+kaolinite and potash-feldspar+muscovite+quartz buffers. Thin dashed lines represent dolomite (dol) and calcite (cal) buffers (activities same as in Fig. 2). The effect of change in the activity of dissolved sulfur species on the solubility is shown through the shift in the position of 100 ppm solubility contour which moves towards higher pH region on decreasing the activity of dissolved sulfur species from $1x10^{-2}$ (thick lines) to $1x10^{-5}$ (thin lines)., a) solubility of ZnS, b) solubility of PbS.

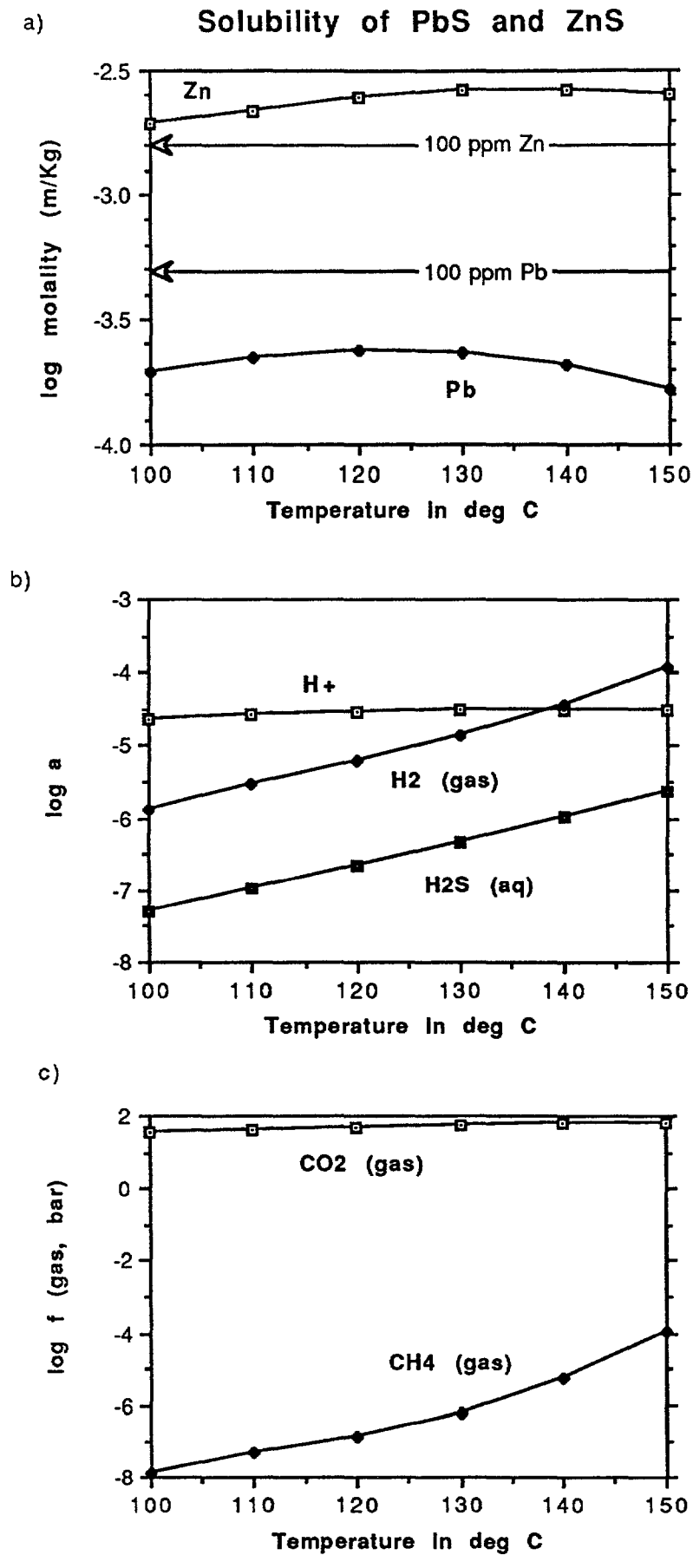

Fig 4. Solubility of PbS and ZnS in a saline fluid (Fluid A) buffered by the chloritized and dolomitized rock (Table 3). The curves represent log molality of all the aqueous species of lead and zinc. Through out this temperature range $PbCl_3^-$, $PbCl_4^{-2}$ and $ZnCl_3^-$, $ZnCl_4^{-2}$ are the dominant species of lead and zinc respectively. The pH of the fluid is buffered by dolomite and the redox state by the pyrite-magnetite assemblage. The activities of reduced sulfur species are controlled by pyrite.

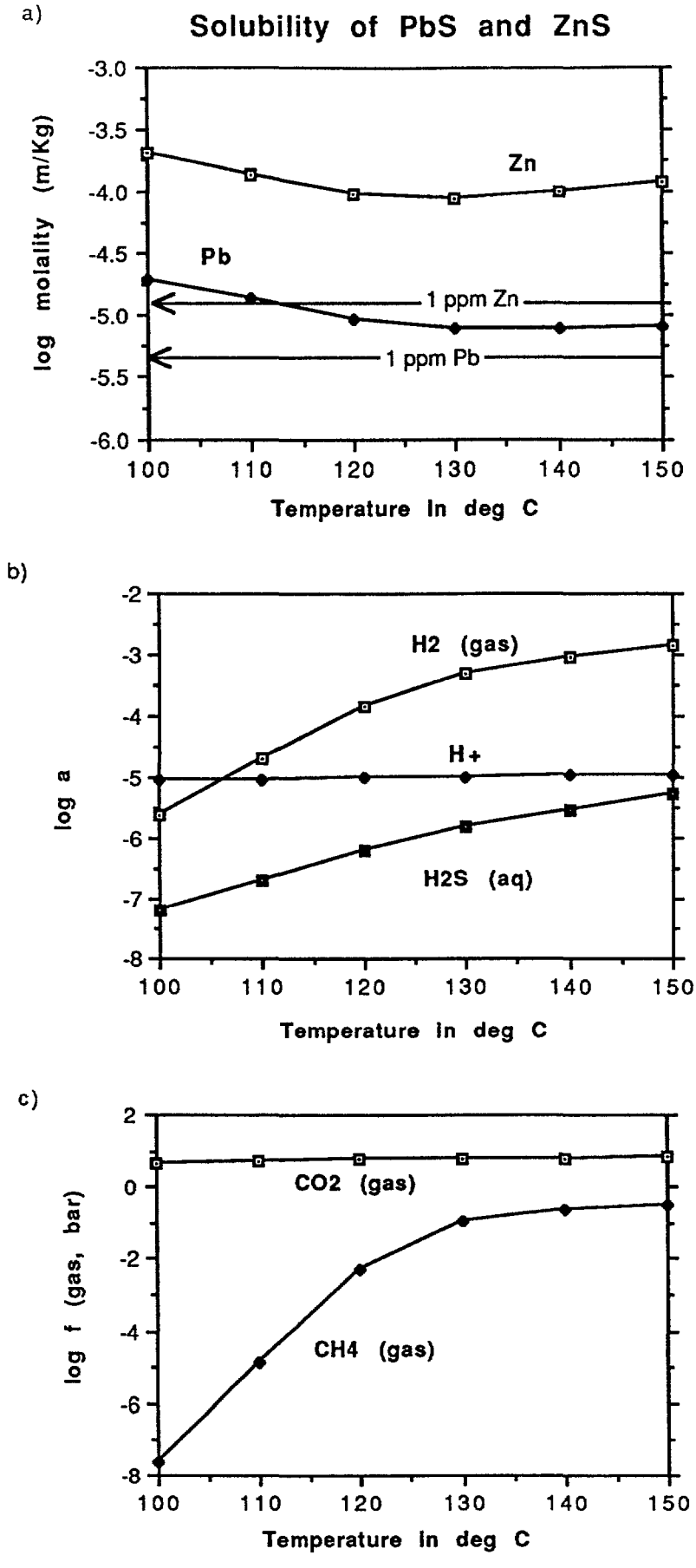

Fig. 5 Solubility of PbS and ZnS in a saline fluid (Fluid A) buffered by the chloritized and dolomitized rock (Table 3). the fluid has 100 times lower concentration of CO_2 (0.06m instead of 0.6m). The curves represent log molality of all the aqueous species of lead and zinc. Buffering conditions same as is Fig. 4. The activities of reduced sulfur species are controlled by pyrite.

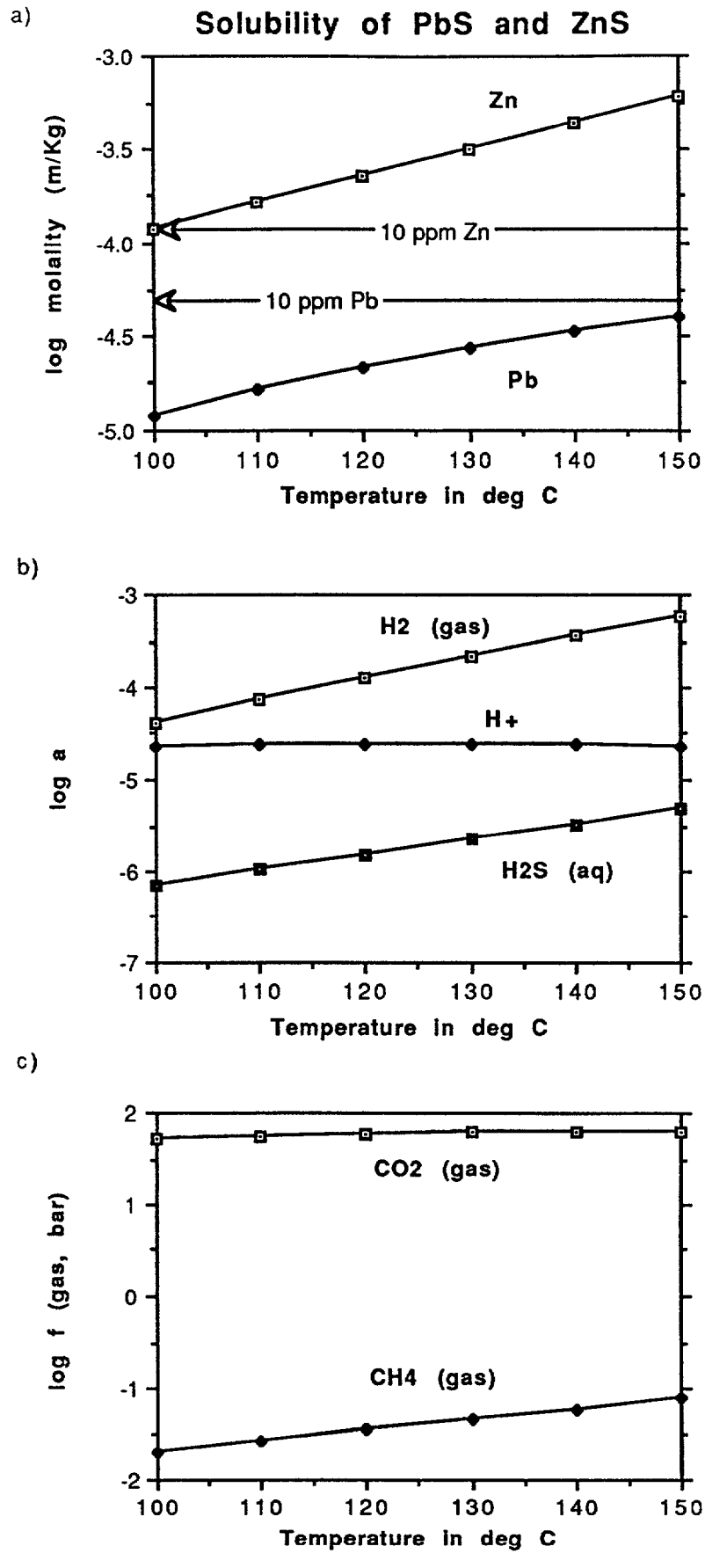

Fig. 6 Solubility of PbS and ZnS in a saline fluid (Fluid A) buffered by siliceous dolostone.(Table 3). The curves represent logmolality of all the aqueous species of lead and zinc. The pH of the fluid is buffered by dolomite and the redox state by the CO_2/CH_4 pair. The activities of reduced sulfur species are controlled by pyrite.

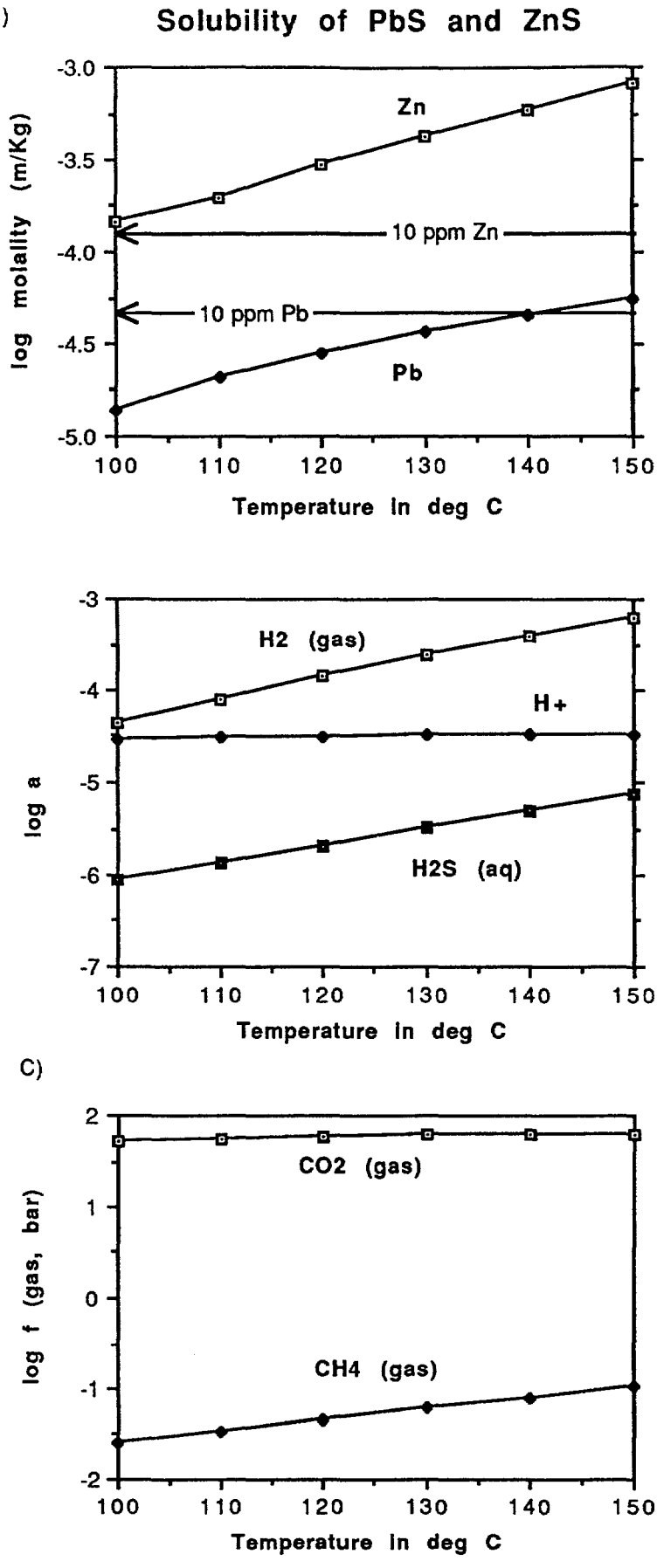

Fig. 7 Solubility of PbS and ZnS in a saline fluid (Fluid B) buffered by siliceous limestone(Table 3). The curves represent logmolality of all the aqueous species of lead and zinc. The pH of the fluid is buffered by calcite and the redox state by the CO_2/CH_4 pair. The activities of reduced sulfur species are controlled by pyrite.

a)

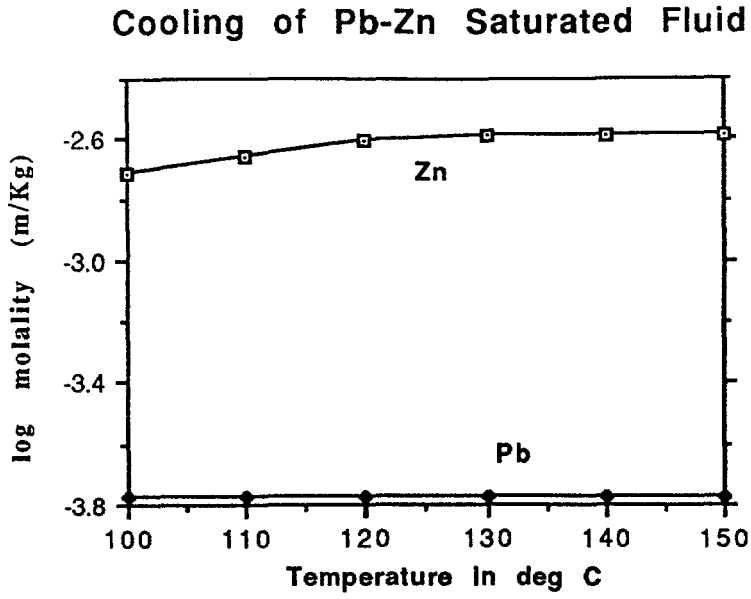

b)

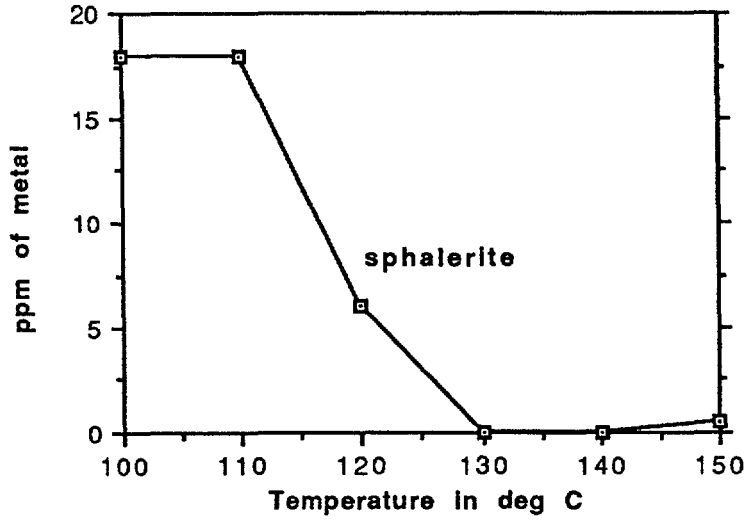

c)

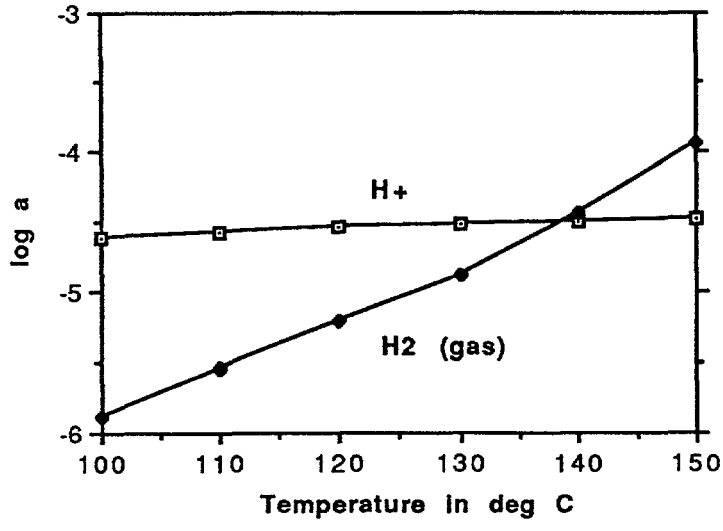

Fig. 8 Cooling of a fluid saturated in lead and zinc at 150°C in equilibrium with an excess of chloritized and dolomitized rock (Fluid/rock ratio of 1:50). The fluid remains undersaturated with respect to galena. Sphalerite precipitates between 150°C and 140°C but dissolves and starts reprecipitating below 130°C . The amount of sphalerite precipitated is expressed in ppm of zinc.

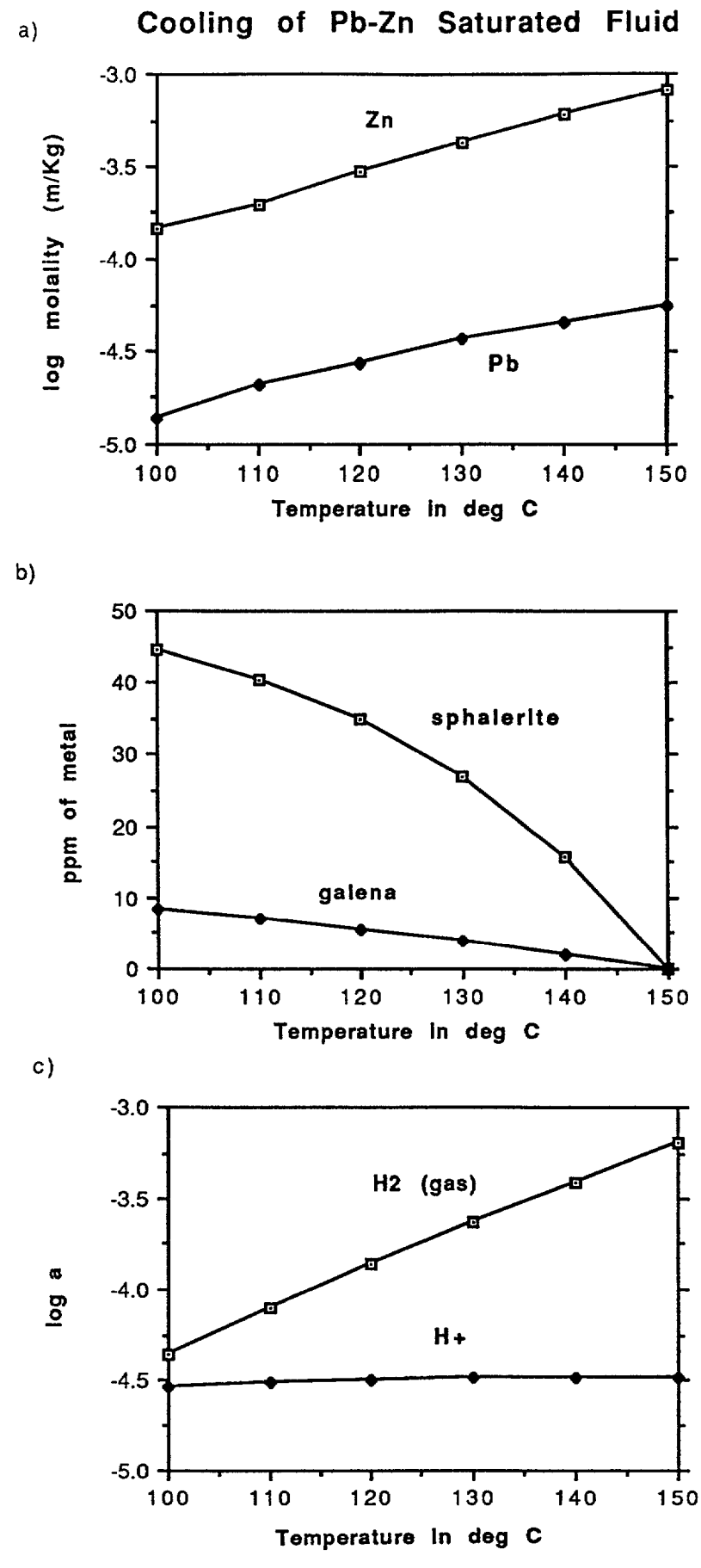

Fig. 9 Cooling of a fluid saturated in lead and zinc at 150°C in equilibrium with an excess of siliceous dolostone (Fluid/rock ratio of 1:50). Sphalerite and galena start precipitating immediately below 150°C and on reaching 100°C, 75% of dissolved lead and 84% of zinc is deposited as galena and sphalerite. The amount of sphalerite and galena precipitated is expressed in ppm of zinc and lead. During cooling the fluid becomes progressively undersaturated in pyrite leading to its dissolution (not shown in the figiure).

a) Cooling of Pb-Zn Undersaturated Fluid

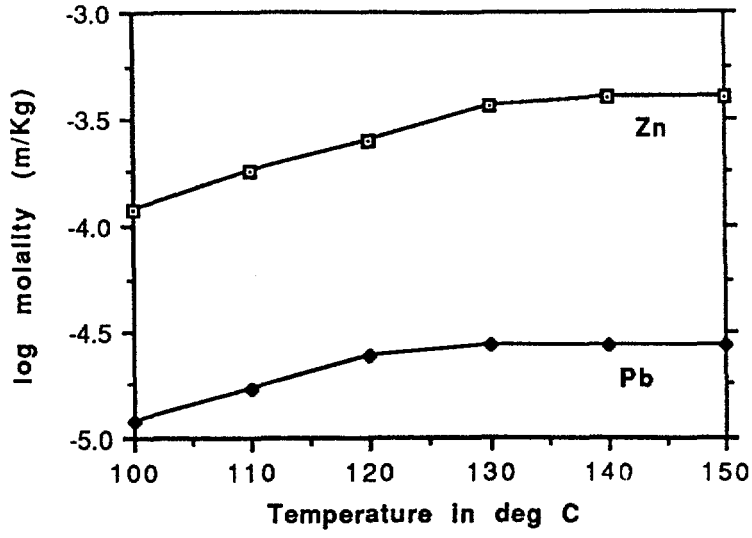

b)

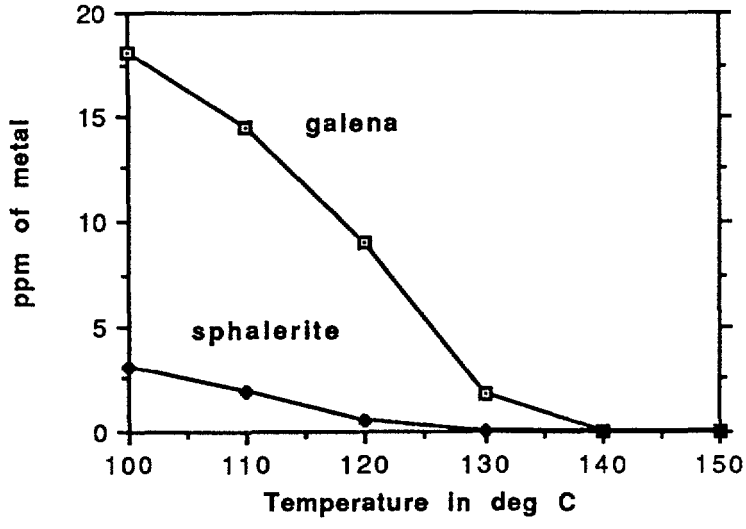

c)

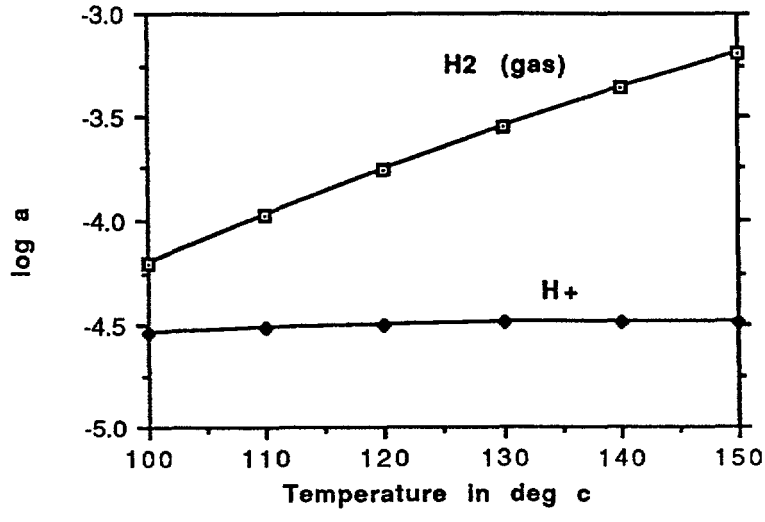

Fig.10 Cooling of a fluid undersaturated in lead and zinc at 150°C in equilibrium with an excess of siliceous dolostone (Fluid/rock ratio of 1:50). Sphalerite starts precipitating below 140°C followed by galena below 130°C . On reaching 100°C , 56% of dissolved lead and 70% of zinc is deposited as galena and sphalerite. The amount of sphalerite and galena precipitated is expressed in ppm of zinc and lead. During cooling the fluid becomes progressively undersaturated in pyrite leading to its dissolution (not shown in the figure.).

a)

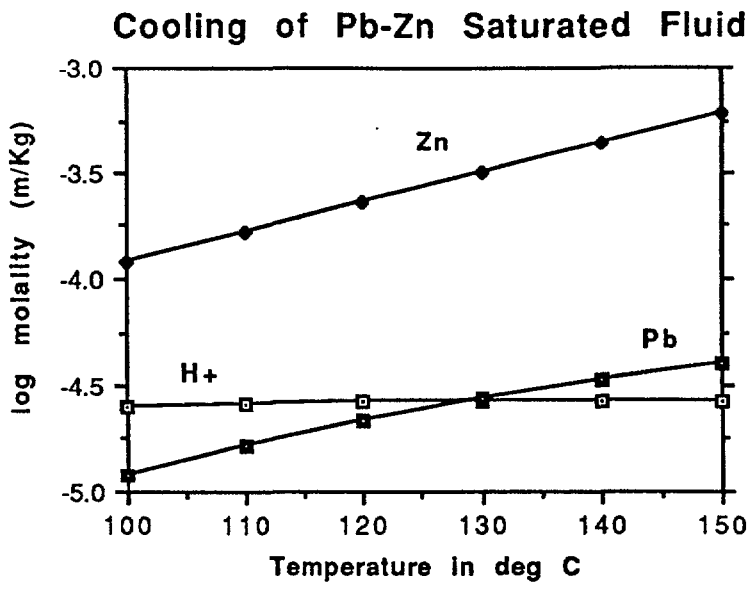

b)

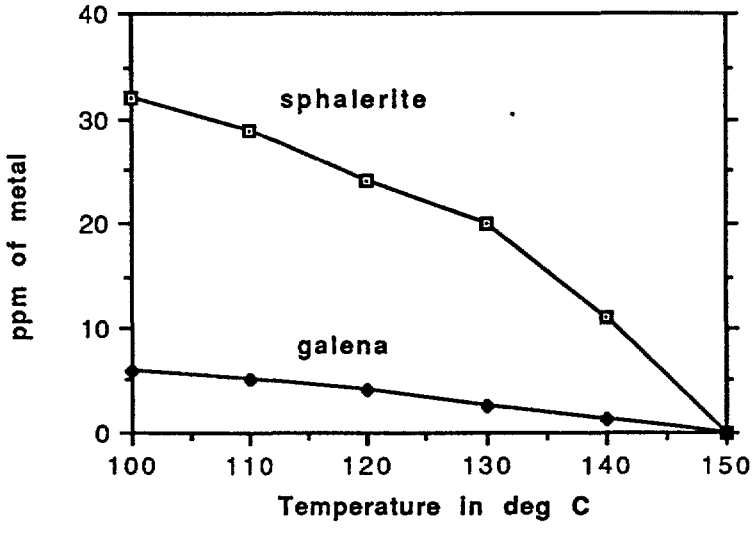

Fig.11 Cooling of a fluid saturated in lead and zinc at 150°C in equilibrium with an excess of siliceous limestone (Fluid/rock ratio of 1:5). Sphalerite and galena start precipitating immediately below 150°C . On reaching 100°C , 70% of dissolved lead and 80% of zinc is deposited as galena and sphalerite. The amount of sphalerite and galena precipitated is expressed in ppm of zinc and lead. During cooling the fluid becomes progressively undersaturated in pyrite and calcite leading to their dissolution (not shown in the figure).

a)

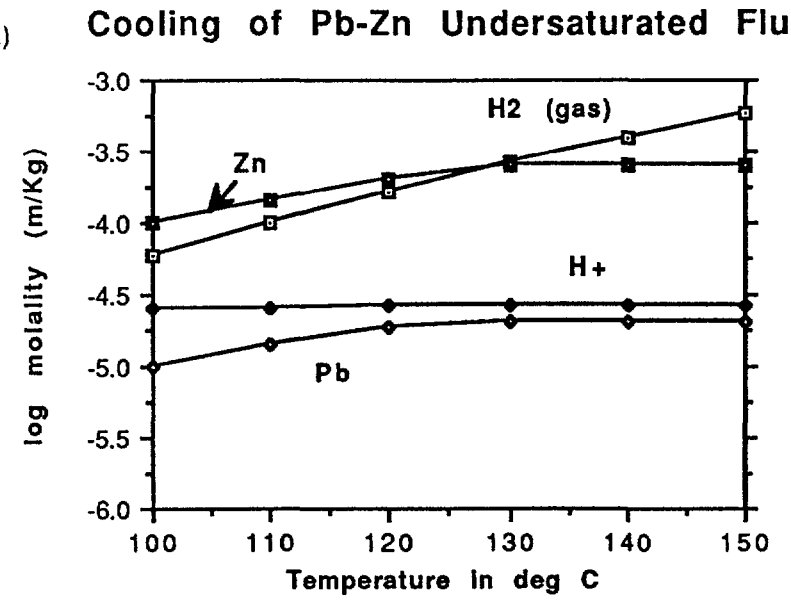

b)

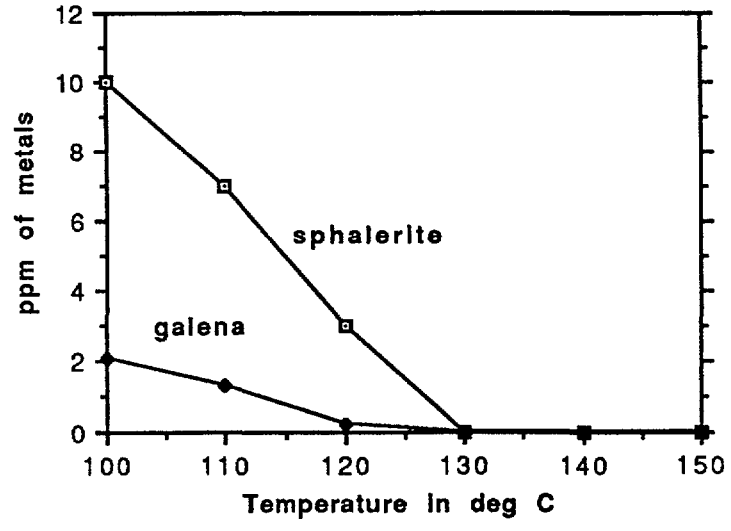

Fig.12 Cooling of a fluid undersaturated in lead and zinc at 150°C in equilibrium with an excess of siliceous limestone(Fluid/rock ratio of 1:5). Sphalerite and galena start precipitating below 130°C . On reaching 100°C , 50% of dissolved lead and 60% of zinc is deposited as galena and sphalerite. Amount of sphalerite and galena precipitated is expressed in ppm of zinc and lead. During cooling the fluid becomes progressively undersaturated in pyrite and calcite leading to their dissolution (not shown in the figure).

a)

Reaction with Limestone

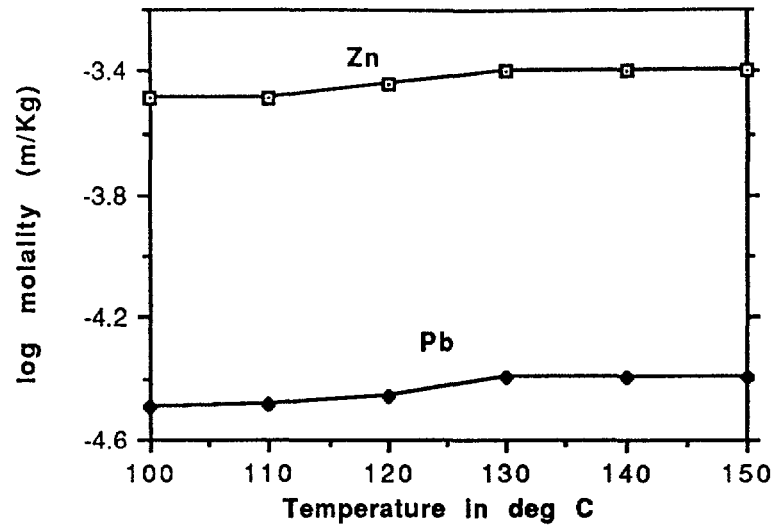

b)

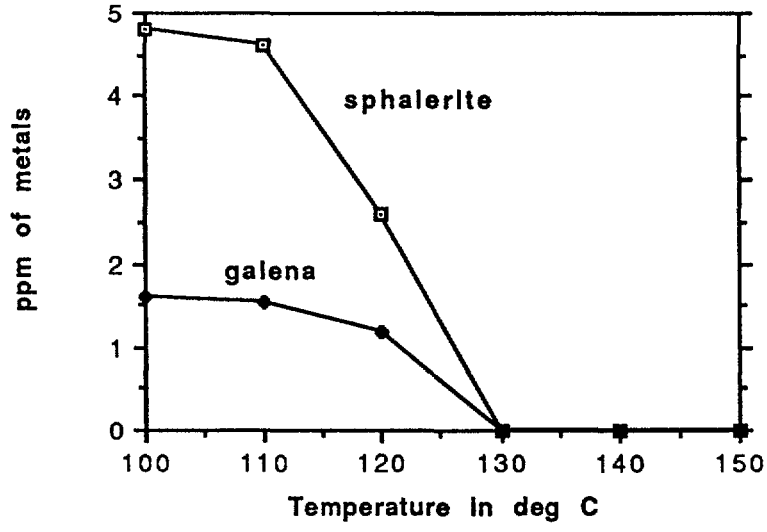

c)

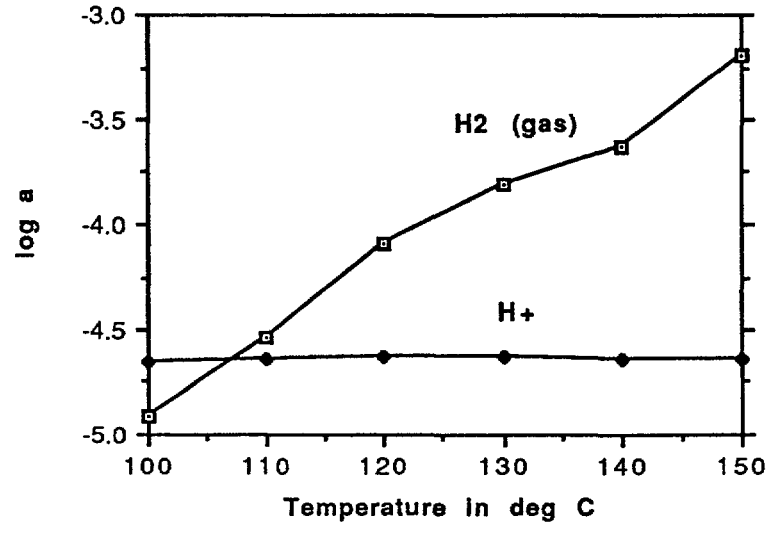

Fig. 13 Reaction of a fluid, initially undersaturated in lead and zinc and buffered by chloritized and dolomitized rock at 150°C, with fresh siliceous limestone at decreasing temperature (fluid/rock ratio of 1:10 at each step). In this type of calculation, 1Kg of the fluid is equilibrated at each temperature with 10 Kg of fresh siliceous limestone. Concentration of total dissolved lead and zinc in the fluid, log activity of H^+ and log fugacity of $H_2(g)$ and the ppm of metal precipitated due to the reaction at each temperature are plotted in the figure. At each temperature part of the limestone is dolomitized (see text for details). The precipitation of galena and sphalerite due to the reaction with limestone begins at temperatures below 130°C. At higher temperatures the fluid in spite of the reaction remains undersaturated in galena and sphalerite despite fluid-rock reaction.

a)

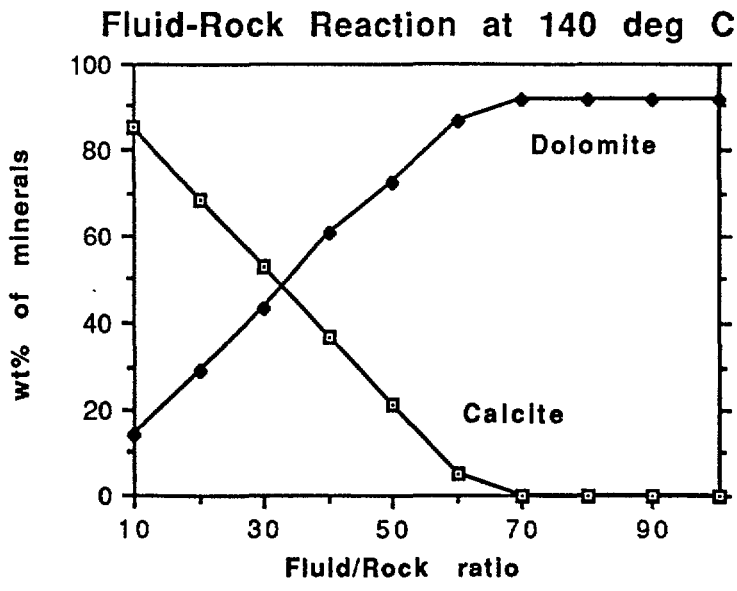
Fluid-Rock Reaction at 140 deg C
wt% of minerals
100
80
60
40
20
0
10
30
50
70
90
Fluid/Rock ratio
Dolomite
Calcite

b)

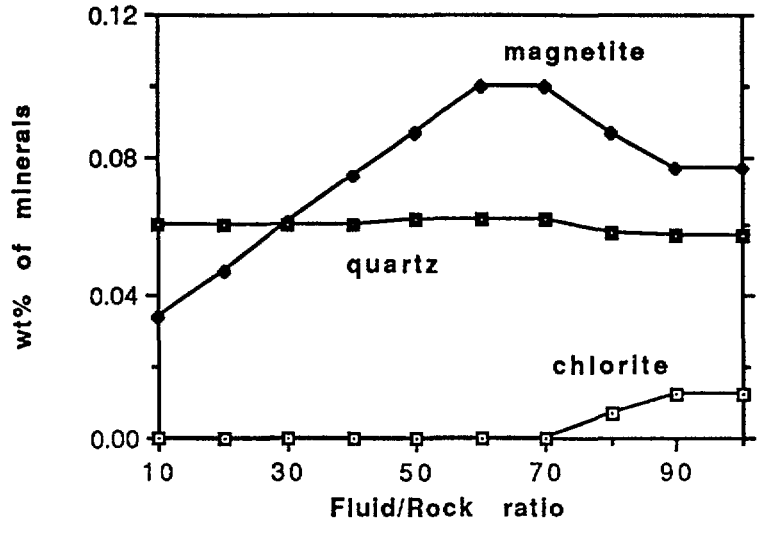
wt% of minerals
0.12
0.08
0.04
0.00
10
30
50
70
90
Fluid/Rock ratio
magnetite
quartz
chlorite

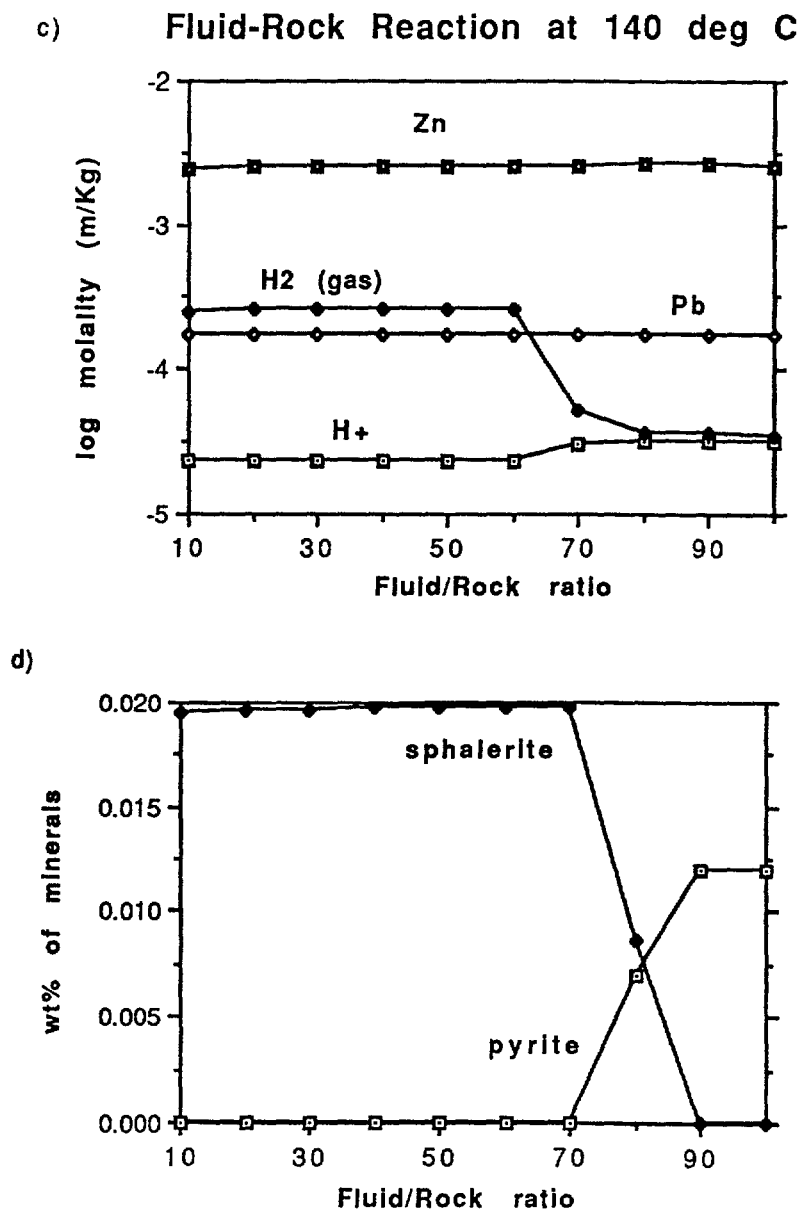

Fig. 14 Stepwise reaction of a fluid saturated in lead and zinc and buffered by the chloritized and dolomitized rock at 150°C with fresh pyrite-bearing siliceous limestone at 140°C . In these calculations, 10 Kg of the fluid reacts with 0.1 Kg of the rock. The calculations represent a system in which the fluid is divided into ten equal batches and each batch successively reacts with the same rock progressively altering it. The first batch of the fluid reacts with the rock, alters it and flows past, followed by the subsequent batches of the same fluid. The fluid/rock ratios marked on the x-axis of each diagram represent growing intensity of interaction of the rock with the fluid and the intensity of its alteration (see text for explanation). The fluid remains undersaturated in galena throughout the process. Sphalerite is precipitated in the earlier stages but after the complete removal of calcite from the system and reappearance of pyrite, chlorite starts dissolving and disappears completely.

a)

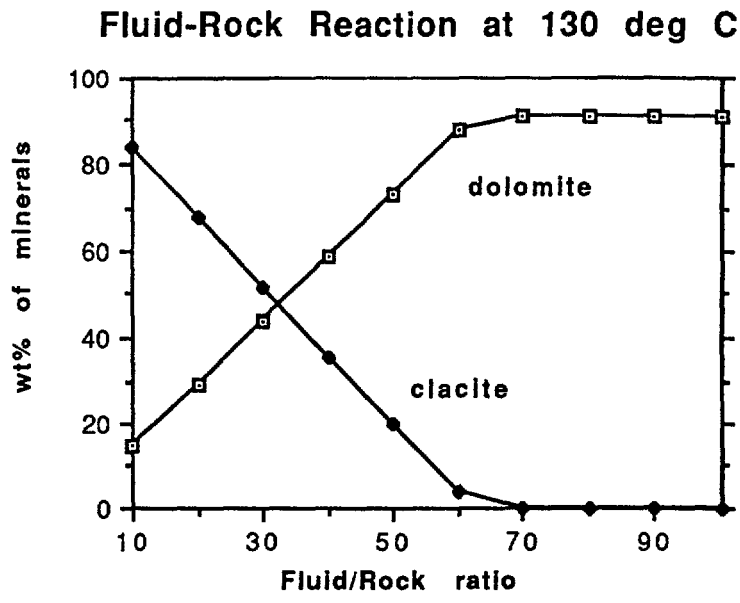
Fluid-Rock Reaction at 130 deg C
wt% of minerals
100
80
60
40
20
0
10
30
50
70
90
Fluid/Rock ratio
dolomite
clacite

b)

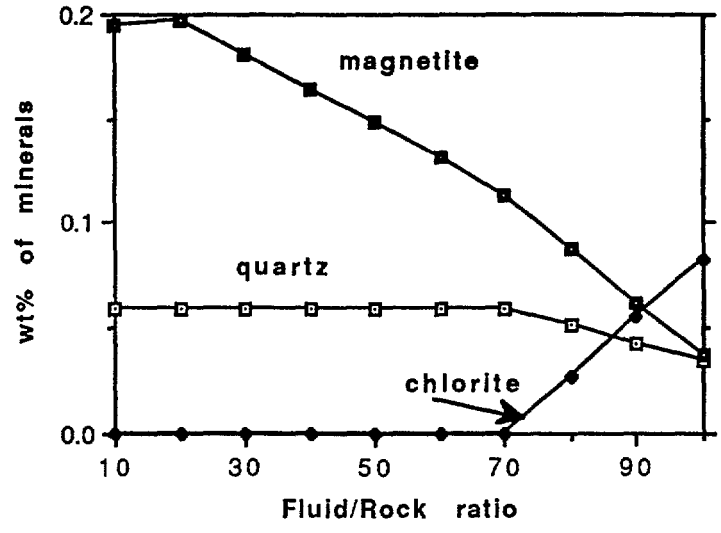
wt% of minerals
0.2
0.1
0.0
10
30
50
70
90
Fluid/Rock ratio
magnetite
quartz
chlorite

a)

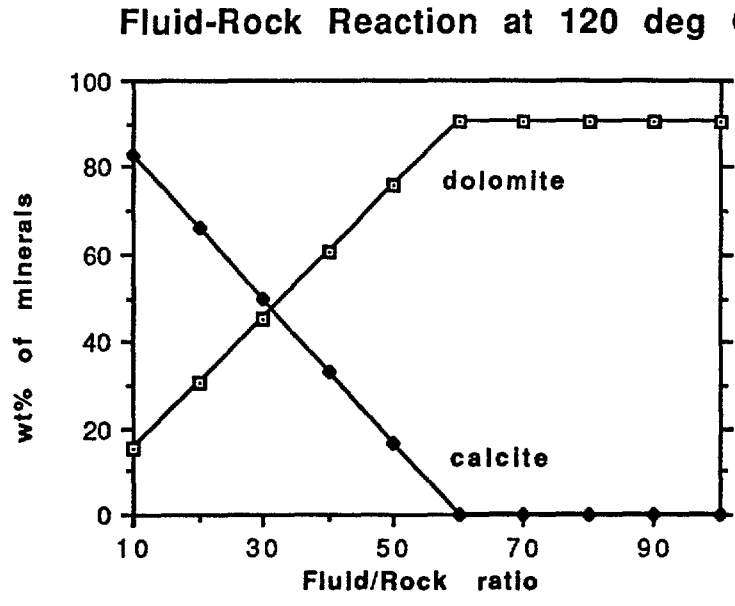
Fluid-Rock Reaction at 120 deg C
wt% of minerals
100
80
60
40
20
0
10
30
50
70
90
Fluid/Rock ratio
dolomite
calcite

b)

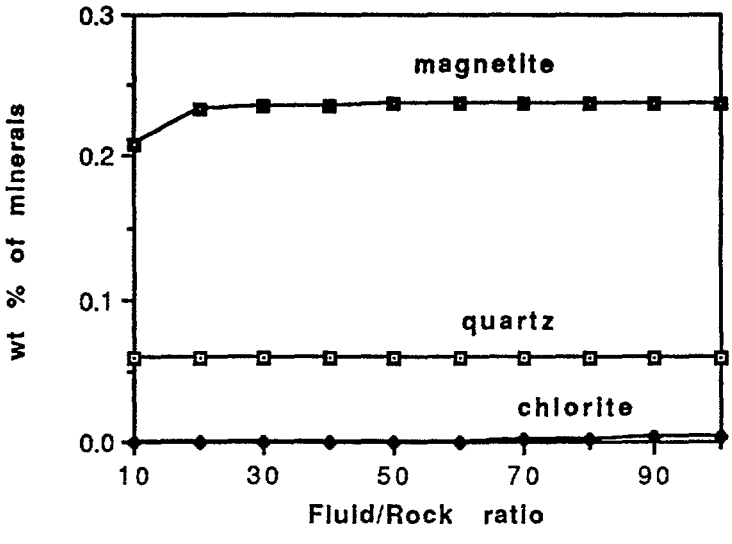
wt % of minerals
0.3
0.2
0.1
0.0
10
30
50
70
90
Fluid/Rock ratio
magnetite
quartz
chlorite

c)

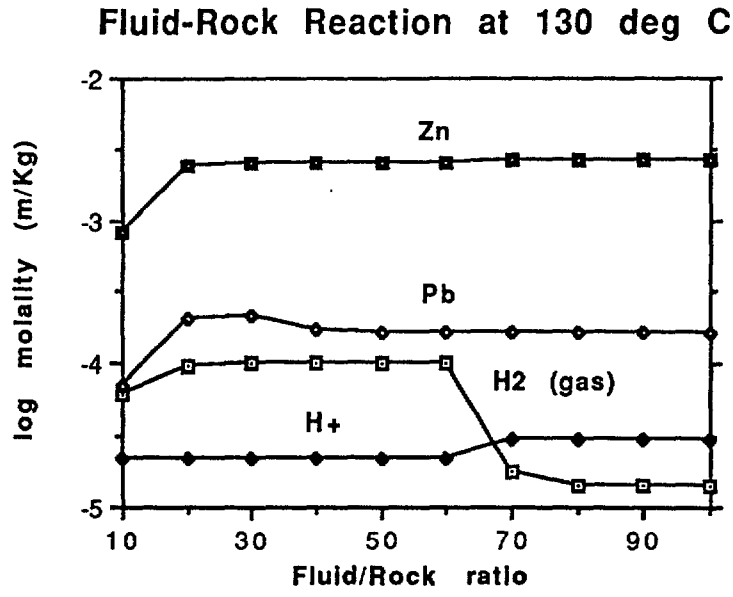

d)

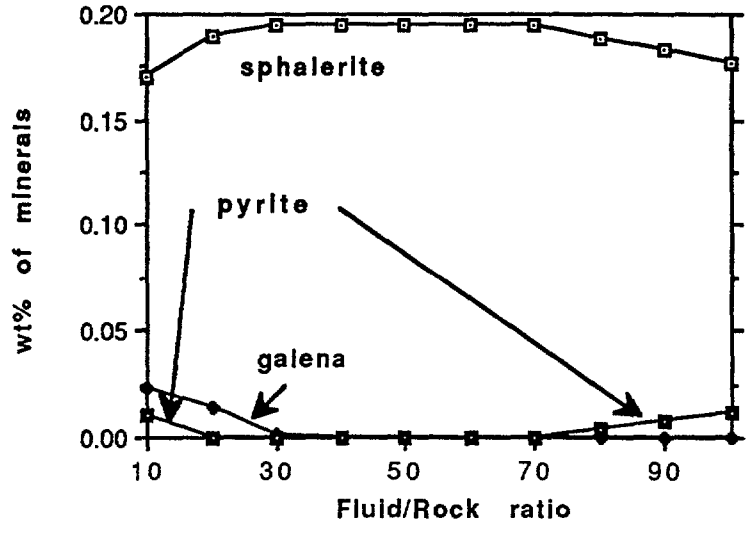

Fig. 15 Same as in Fig 14. Fluid-rock reaction at 130°C . The fluid precipitates galena in the earlier stages but dissolves completely above the fluid/rock ratio of 30. Sphalerite is precipitated in the earlier stages but after the complete removal of calcite from the system and the reappearance of pyrite and chlorite, it starts dissolving.

c)

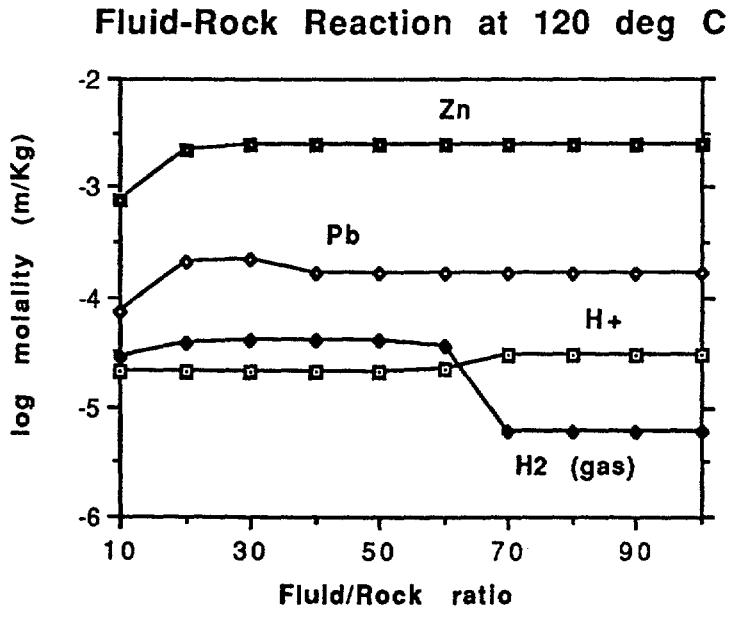

d)

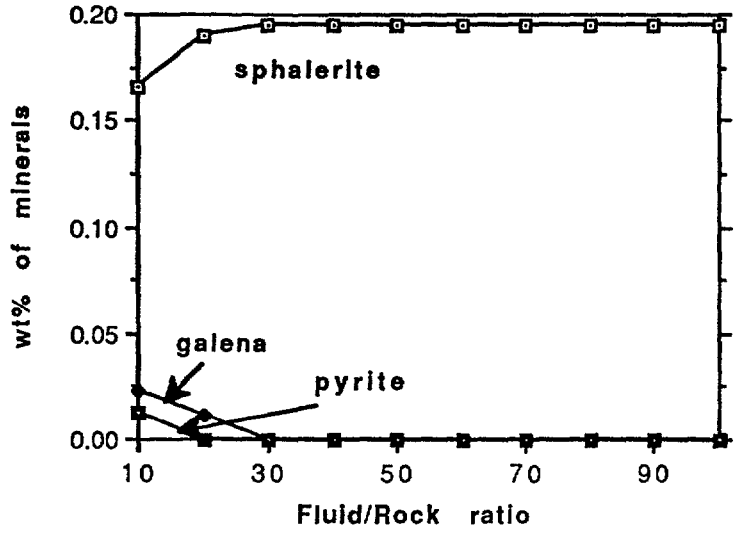

Fig. 16 Same as in Fig 14. Fluid-rock reaction at 120°C . The fluid precipitates galena in the earlier stages but dissolves completely above the fluid/rock ratio of 30. With respect to sphalerite the fluid remains saturated throughout causing continuous deposition. Pyrite dissolves completely above fluid/rock ratio of 30 but starting from the fluid/rock ratio of 70 it reappears in very small amount ($3x10^{-5}$ to $1x10^{-4}$wt %), difficult to be depicted in the diagram 16d.

a)

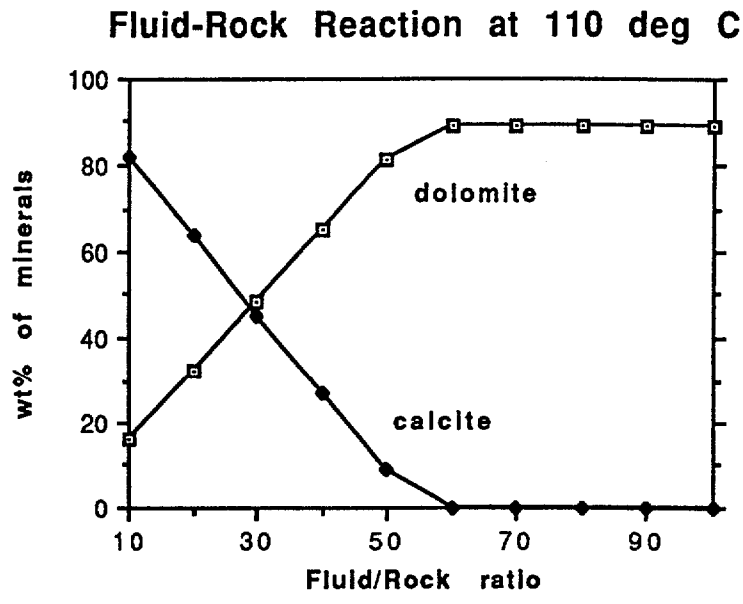
Fluid-Rock Reaction at 110 deg C
wt% of minerals
100
80
60
40
20
0
10
30
50
70
90
Fluid/Rock ratio
dolomite
calcite

b)

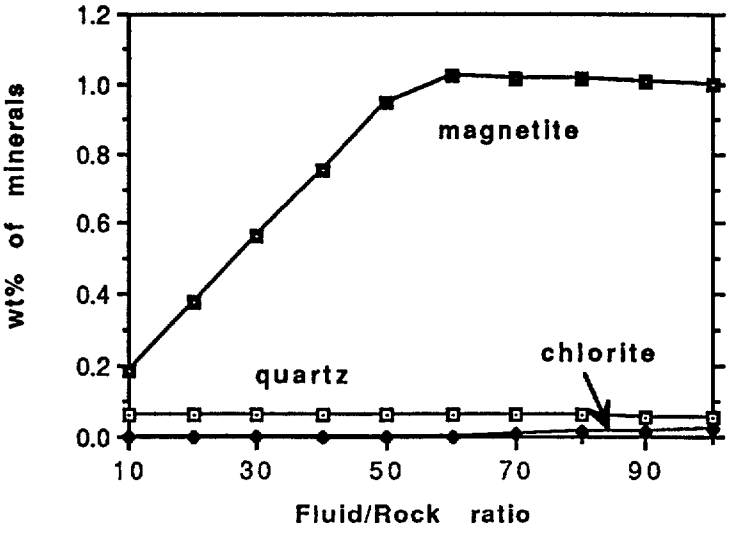
wt% of minerals
1.2
1.0
0.8
0.6
0.4
0.2
0.0
10
30
50
70
90
Fluid/Rock ratio
magnetite
quartz
chlorite

c)

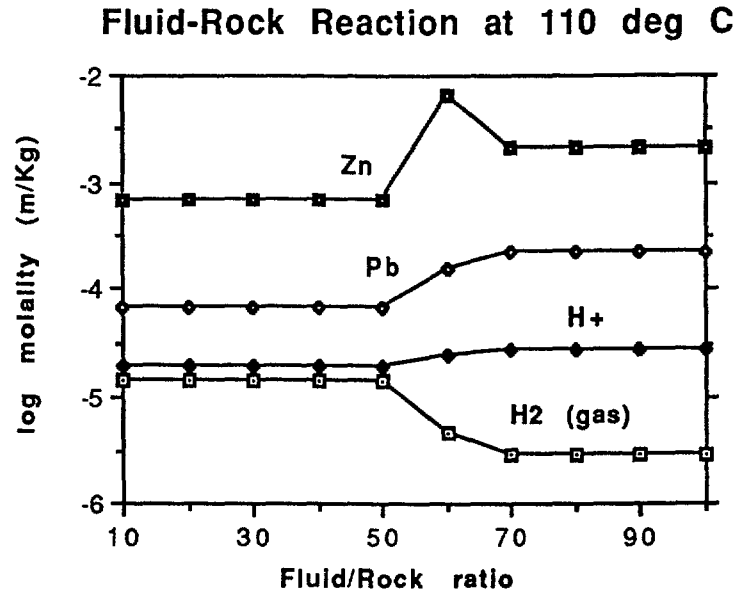

d)

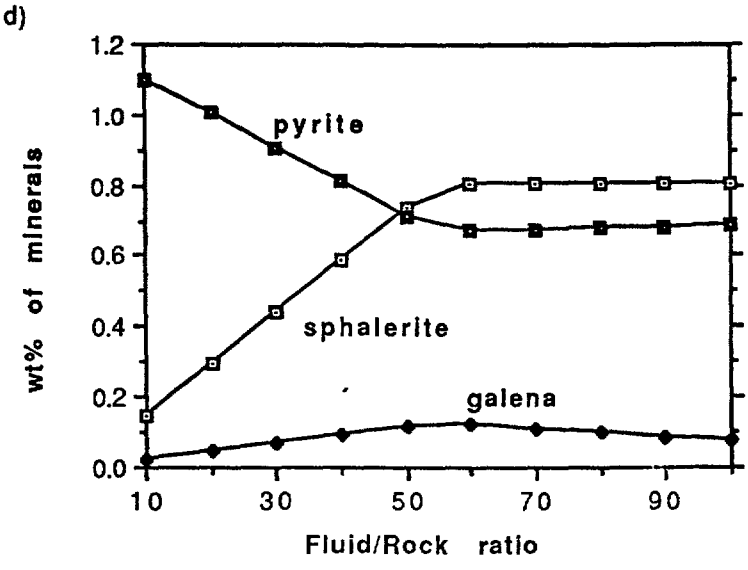

Fig. 17 Same as in Fig 14. Fluid-rock reaction at 110°C . The fluid precipitates galena in the earlier stages but starts dissolving slightly above the fluid/rock ratio of 60. With respect to sphalerite the fluid remains saturated throughout causing its continuous deposition.

a)

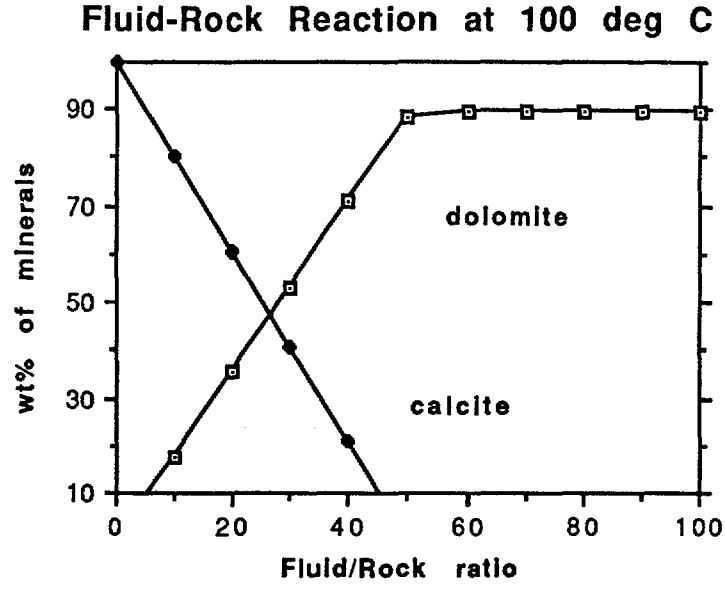
Fluid-Rock Reaction at 100 deg C
wt% of minerals
90
70
50
30
10
0
20
40
60
80
100
Fluid/Rock ratio
dolomite
calcite

b)

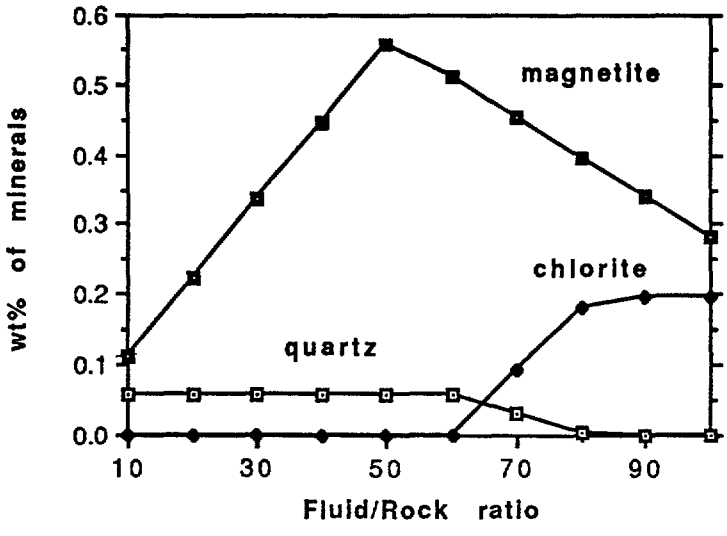
wt% of minerals
0.6
0.5
0.4
0.3
0.2
0.1
0.0
10
30
50
70
90
Fluid/Rock ratio
magnetite
chlorite
quartz

c)

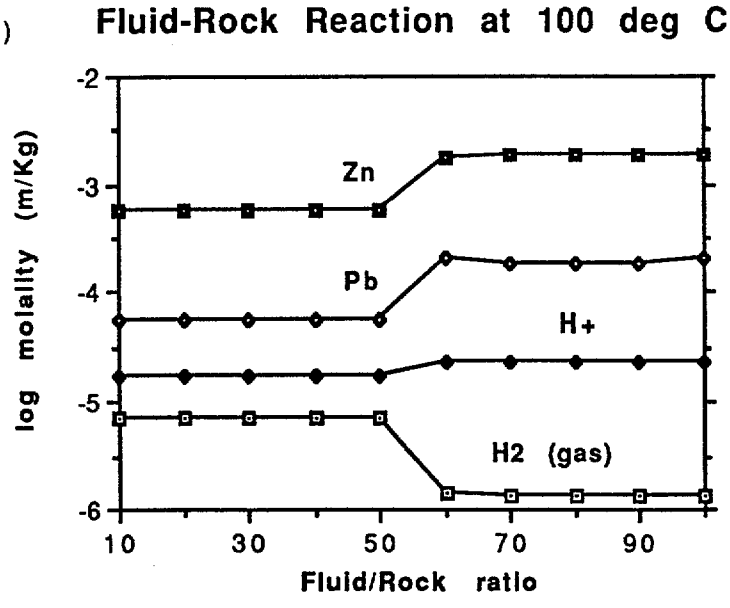

d)

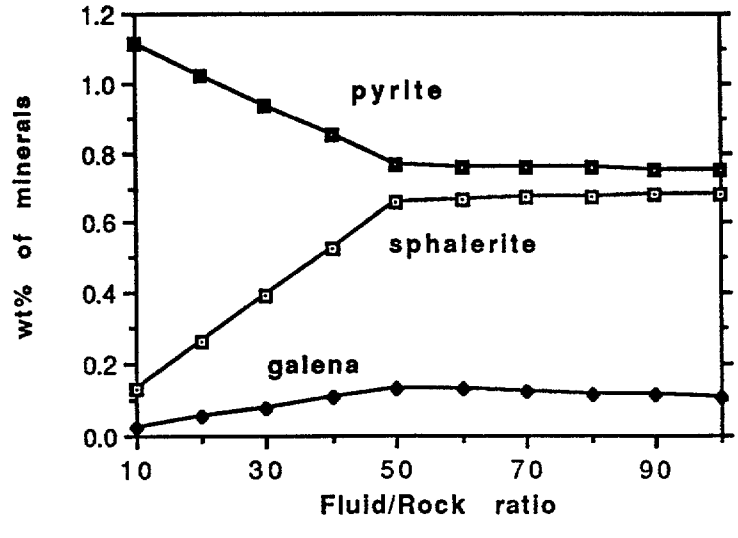

Fig. 18 Same as in Fig 14 Fluid-rock reaction at 100°C The fluid precipitates galena in the earlier stages but starts dissolving slightly above the fluid/rock ratio of 60. With respect to sphalerite the fluid remains saturated throughout causing its continuous deposition.

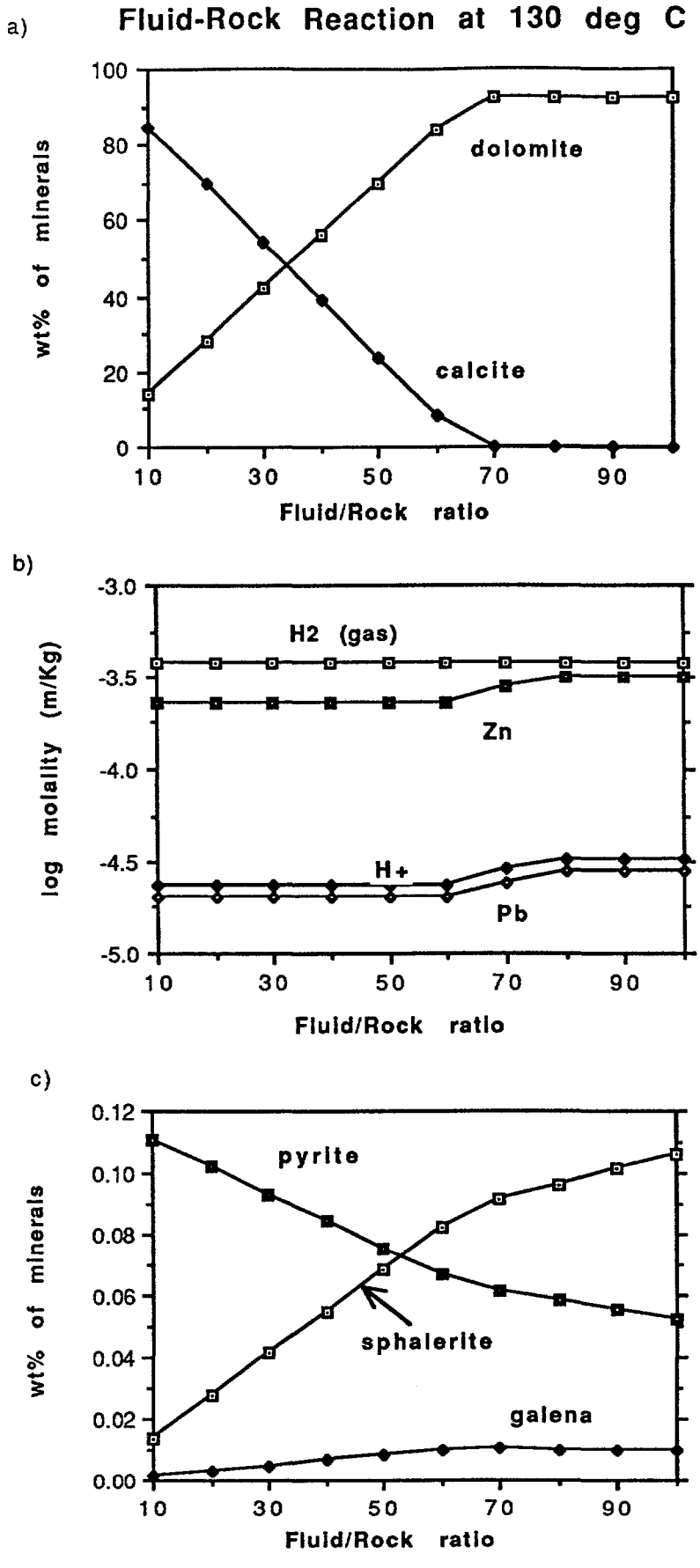

Fig. 19 Same as in Fig 14. Fluid-rock reaction at 100°C . The fluid is undersaturated in lead and zinc at 150°C and is buffered by a siliceous dolostone (Table 2). This fluid precipitates galena in the earlier stages but starts dissolving it in minor amounts above thefluid/rock ratio of 60. With respect to sphalerite the fluid remains saturated throughout, causing its continuous deposition.

APPENDIX: Thermodynamic Data

H2 O (G) SOURCE CPDMRLDAT DATA TYPE CPD
hydrogen oxide gas water steam

DHF(298) = -57798.0 CAL S(298) = 45.106 CAL /K
CP = 6.92691 + (0.264398E-02*T) + (0.255648E-06*T*T) + (25572.3 /T/T)
TMAX = 1000.00 K DH(TMAX) = 0.0 CAL
CP = 5.81776 + (0.484525E-02*T) + (-.823864E-06*T*T) + (0.000000E+00/T/T)
TMAX = 2000.00 K DH(TMAX) = 0.0 CAL

H2 (G) SOURCE CPDMRLDAT DATA TYPE CPD
hydrogen diatomic gas

DHF(298) = 0.0 CAL S(298) = 31.207 CAL /K
CP = 7.18062 + (-.592740E-03*T) + (0.641294E-06*T*T) + (-14285.2 /T/T)
TMAX = 1500.00 K DH(TMAX) = 0.0 CAL
CP = 7.46736 + (0.580198E-03*T) + (-.226250E-07*T*T) + (-.132201E+07/T/T)
TMAX = 6000.00 K DH(TMAX) = 0.0 CAL

O2 (G) SOURCE CPDMRLDAT DATA TYPE CPD
oxygen diatomic gas

DHF(298) = 0.0 CAL S(298) = 49.005 CAL /K
CP = 5.53715 + (0.435479E-02*T) + (-.157390E-05*T*T) + (28541.0 /T/T)
TMAX = 1200.00 K DH(TMAX) = 0.0 CAL
CP = 7.54918 + (0.877266E-03*T) + (-.709300E-07*T*T) + (54195.7 /T/T)
TMAX = 6000.00 K DH(TMAX) = 0.0 CAL

C O2 (G) SOURCE CPDMRLDAT DATA TYPE CPD
carbon dioxide gas

DHF(298) = -94054.0 CAL S(298) = 51.072 CAL /K
CP = 10.5700 + (0.210000E-02*T) + (0.000000E+00*T*T) + (-206000. /T/T)
TMAX = 2500.00 K DH(TMAX) = 0.0 CAL

C H4 (G) SOURCE CPDMRLDAT DATA TYPE CPD
methane gas

DHF(298) = -17880.0 CAL S(298) = 44.492 CAL /K
CP = 1.47373 + (0.212384E-01*T) + (-.566260E-05*T*T) + (105927. /T/T)
TMAX = 1500.00 K DH(TMAX) = 0.0 CAL

H2 S (G) SOURCE CPDMRLDAT DATA TYPE CPD
hydrogen sulphide gas

DHF(298) = -4880.0 CAL S(298) = 49.151 CAL /K
CP = 7.81000 + (0.296000E-02*T) + (0.000000E+00*T*T) + (-46000.0 /T/T)
TMAX = 2300.00 K DH(TMAX) = 0.0 CAL

S O2 (G) SOURCE CPDMRLDAT DATA TYPE CPD
sulphur dioxide gas

DHF(298) = -70947.0 CAL S(298) = 59.298 CAL /K
CP = 11.0400 + (0.188000E-02*T) + (0.000000E+00*T*T) + (-184000. /T/T)
TMAX = 2000.00 K DH(TMAX) = 0.0 CAL

H CL (G) SOURCE CPDMRLDAT DATA TYPE CPD
hydrogen chloride gas

DHF(298) = -22063.0 CAL S(298) = 44.645 CAL /K
CP = 6.27000 + (0.124000E-02*T) + (0.000000E+00*T*T) + (30000.0 /T/T)
TMAX = 2000.00 K DH(TMAX) = 0.0 CAL

H2 O SOURCE GIBBMRAQU DATA TYPE GIB
water liquid mrl(25-300;l/v); bhd(350-600 rho=1.74)

A	B	C	D	E	F
-284433.	4184.71	0.857524	-.195525E-03	0.124675E+08	-666.839

TMIN = 298.15 K TMAX = 873.15 K

H2 (AQ) SOURCE GIBBMRAQU DATA TYPE GIB
h2 aq.

A	B	C	D	E	F
-.739908E+07	157988.	39.9084	-.112762E-01	0.385274E+09	-26044.0

TMIN = 298.15 K TMAX = 573.15 K

O2 (AQ) SOURCE GIBBMRAQU DATA TYPE GIB
o2 aqueous

A	B	C	D	E	F
381033.	-6972.54	-1.24958	0.167179E-03	-.229679E+08	1109.92

TMIN = 298.15 K TMAX = 573.15 K

C O2 (AQ) SOURCE GIBBMRAQU DATA TYPE GIB
drummond

A	B	C	D	E	F
-107912.	230.917	0.000000E+00	0.000000E+00	0.000000E+00	-31.3470

TMIN = 298.15 K TMAX = 673.15 K

C H4 (AQ) SOURCE GIBBMRAQU DATA TYPE GIB
drummond

A	B	C	D	E	F
-33169.7	317.376	0.000000E+00	0.000000E+00	0.000000E+00	-40.9972

TMIN = 298.15 K TMAX = 673.15 K

H2 S (AQ) SOURCE GIBBMRAQU DATA TYPE GIB
hydrogen sulphide aqueous, drummond

A	B	C	D	E	F
-10418.6	61.9232	0.000000E+00	0.000000E+00	0.000000E+00	-8.56774

TMIN = 298.15 K TMAX = 673.15 K

S O2 (AQ) SOURCE GIBMRLSUB DATA TYPE GIB
thrlwfit based on henry law const from drummond (1981) table 3.6

A	B	C	D	E	F
-151239.	1142.89	0.000000E+00	0.000000E+00	0.000000E+00	-154.217

TMIN = 298.15 K TMAX = 623.15 K

H E-1 (AQ) SOURCE GIBBMRAQU DATA TYPE GIB
hydrogen ion aqueous

A	B	C	D	E	F
0.000000E+00	0.000000E+00	0.000000E+00	0.000000E+00	0.000000E+00	0.0E+00

TMIN = 298.15 K TMAX = 873.15 K

O H E1 (AQ) SOURCE GIBBMRAQU DATA TYPE GIB
oh-

A	B	C	D	E	F
0.500857E+07	-114641.	-31.8212	0.983694E-02	-.247866E+09	19151.5

TMIN = 298.15 K TMAX = 623.15 K

CL E1 (AQ) SOURCE GIBBMRAQU DATA TYPE GIB
chloride ion aqueous mrl refit within 25cal; deviation coblle 100cal
A B C D E F
-27034.1 -253.070 0.000000E+00 0.000000E+00 0.000000E+00 41.8742
TMIN = 298.15 K TMAX = 623.15 K

H CL (AQ) SOURCE GIBMRLCHR DATA TYPE GIB
hcl r/s constant dcp fit
A B C D E F
-91300.7 921.850 0.000000E+00 0.000000E+00 0.000000E+00 -126.742
TMIN = 298.15 K TMAX = 673.15 K

H C O3 E1 (AQ) SOURCE GIBBMRAQU DATA TYPE GIB
bicarbonate ion aqueous, pk cobble et al. 81 p.4-24; drummond for co2
A B C D E F
-151425. -199.260 0.000000E+00 0.000000E+00 0.000000E+00 41.5607
TMIN = 298.15 K TMAX = 673.15 K

C O3 E2 (AQ) SOURCE GIBBMRAQU DATA TYPE GIB
co3--
A B C D E F
0.290537E+08 -657804. -181.169 0.555896E-01 -.144123E+10 109734.
TMIN = 298.15 K TMAX = 623.15 K

H S E1 (AQ) SOURCE GIBBMRAQU DATA TYPE GIB
bisulphide aquieous, pk cubiciotti; h2s drummond
A B C D E F
19048.6 -465.747 0.000000E+00 0.000000E+00 0.000000E+00 72.3136
TMIN = 298.15 K TMAX = 673.15 K

H S O4 E1 (AQ) SOURCE GIBBMRAQU DATA TYPE GIB
bisulphate ion aqueous refit mrl = cobble = cubiciotti
A B C D E F
-196349. -244.993 0.000000E+00 0.000000E+00 0.000000E+00 52.2234
TMIN = 298.15 K TMAX = 573.15 K

S O4 E2 (AQ) SOURCE GIBBMRAQU DATA TYPE GIB
sulphate ion aqu cobble refit within 200cals
A B C D E F
-170997. -840.034 0.000000E+00 0.000000E+00 0.000000E+00 143.451
TMIN = 298.15 K TMAX = 623.15 K

K E-1 (AQ) SOURCE GIBBMRAQU DATA TYPE GIB
potassium ion aqu cobble etal. 81 within 200cals
A B C D E F
-56411.8 -91.6512 0.000000E+00 0.000000E+00 0.000000E+00 9.44631
TMIN = 298.15 K TMAX = 623.15 K

K CL (AQ) SOURCE GIBBMRAQU DATA TYPE GIB
kcl
A B C D E F
-.112175E+08 256385. 72.5980 -.226503E-01 0.531597E+09 -42947.7
TMIN = 298.15 K TMAX = 573.15 K

K O H (AQ) SOURCE GIBMRLCHR DATA TYPE GIB
data from lukashov et al. (1976) cp=0 fit data for 579-638k
A B C D E F
-86046.4 -17.3957 0.000000E+00 0.000000E+00 0.000000E+00 0.000000E+00
TMIN = 298.15 K TMAX = 673.15 K

NA E-1 (AQ) SOURCE GIBBMRAQU DATA TYPE GIB
sodium ion aqu cobble et al.81 within 150cals
A B C D E F
-51895.9 -114.856 0.000000E+00 0.000000E+00 0.000000E+00 13.9030
TMIN = 298.15 K TMAX = 623.15 K

NA CL (AQ) SOURCE GIBBMRAQU DATA TYPE GIB
nacl
A B C D E F
-.204389E+07 43542.5 11.8672 -.360577E-02 0.967901E+08 -7249.44
TMIN = 298.15 K TMAX = 623.15 K

NA O H (AQ) SOURCE GIBMRLCHR DATA TYPE GIB
data from lukashov et al. (1976) cp=0 fit data for 579-638k
A B C D E F
-80477.8 -14.8937 0.000000E+00 0.000000E+00 0.000000E+00 0.000000E+00
TMIN = 298.15 K TMAX = 673.15 K

CA E-2 (AQ) SOURCE GIBBMRAQU DATA TYPE GIB
calcium ion aqu, cobble et al. 81; dont extrapolate
A B C D E F
0.366110E+07 -91488.7 -27.9729 0.944550E-02 -.173100E+09 15482.7
TMIN = 298.15 K TMAX = 573.15 K

CA CL E-1 (AQ) SOURCE GIBBMRAQU DATA TYPE GIB
cacl+
A B C D E F
0.364569E+07 -92021.6 -28.1131 0.949255E-02 -.173559E+09 15574.0
TMIN = 298.15 K TMAX = 623.15 K

CA CL2 (AQ) SOURCE GIBBMRAQU DATA TYPE GIB
cacl2
A B C D E F
0.110728E+07 -35623.1 -12.4342 0.462528E-02 -.495670E+08 6162.63
TMIN = 298.15 K TMAX = 623.15 K

CA O H E-1 (AQ) SOURCE GIBBMRAQU DATA TYPE GIB
caoh+
A B C D E F
0.175191E+07 -47586.4 -14.8121 0.502103E-02 -.857195E+08 8085.74
TMIN = 298.15 K TMAX = 573.15 K

FE E-2 (AQ) SOURCE GIBBMRAQU DATA TYPE GIB
ferrous ion aqueous cobble et al. 81)
A B C D E F
-22816.6 14.9885 0.000000E+00 0.000000E+00 0.000000E+00 -2.08265
TMIN = 298.15 K TMAX = 573.15 K

FE CL E-1 (AQ) SOURCE GIBMRLCHR DATA TYPE GIB
fecl+ isocoloumbic extrapola r/s of zinc 1june 1989
A B C D E F
-136138. 1310.92 0.000000E+00 0.000000E+00 0.000000E+00 -182.965
TMIN = 298.15 K TMAX = 673.15 K

FE CL2 (AQ) SOURCE GIBMRLCHR DATA TYPE GIB
fecl2 (aq) isocoloumbic extrapola using r/s for zinc 1june 1989
A B C D E F
-230274. 2164.80 0.000000E+00 0.000000E+00 0.000000E+00 -296.816
TMIN = 298.15 K TMAX = 673.15 K

MG E-2 (AQ) SOURCE GIBBMRAQU DATA TYPE GIB
magnesium ion aqu, cobble et al. 81; dont extrapolate
A B C D E F
0.507660E+07 -124539. -37.7343 0.126290E-01 -.237900E+09 21053.1
TMIN = 298.15 K TMAX = 573.15 K

MG CL E-1 (AQ) SOURCE GIBBMRAQU DATA TYPE GIB
mgcl+
A B C D E F
0.506121E+07 -125072. -37.8746 0.126761E-01 -.238360E+09 21144.5
TMIN = 298.15 K TMAX = 623.15 K

MG CL2 (AQ) SOURCE GIBMRLSUB DATA TYPE GIB
mgcl2 (aq) based on logkr of disso of cacl2
A B C D E F
-541238. 10915.8 2.28207 0.000000E+00 0.000000E+00 -1816.48
TMIN = 298.15 K TMAX = 623.15 K

AL E-3 (AQ) SOURCE GIBBMRAQU DATA TYPE GIB
alumina ion aqu, refit to mrl, exact
A B C D E F
-129590. 96.0549 0.000000E+00 0.000000E+00 0.000000E+00 -8.86350
TMIN = 298.15 K TMAX = 623.15 K

AL O H E-2 (AQ) SOURCE GIBBMRAQU DATA TYPE GIB
aloh++
A B C D E F
619269. -20115.0 -6.41452 0.210582E-02 -.347585E+08 3439.68
TMIN = 298.15 K TMAX = 573.15 K

AL O2 H2 E-1 (AQ) SOURCE GIBMRLSUB DATA TYPE GIB
al(oh)2+ data refitted from soltherm
A B C D E F
-250377. 368.193 0.000000E+00 0.000000E+00 0.000000E+00 -44.2341
TMIN = 373.15 K TMAX = 573.15 K

AL O4 H4 E1 (AQ) SOURCE GIBBMRAQU DATA TYPE GIB
al(oh)4-
A B C D E F
-.774705E+07 165376. 45.7219 -.142027E-01 0.371239E+09 -27553.0
TMIN = 298.15 K TMAX = 573.15 K

SI O2 (AQ) SOURCE GIBMRLCHR DATA TYPE GIB
silica aqueous backfit to reed's quartz
A B C D E F
-209685. 0.739600 0.000000E+00 0.000000E+00 0.000000E+00 6.00771
TMIN = 298.15 K TMAX = 673.15 K

ZN E-2 (AQ) SOURCE GIBBMRAQU DATA TYPE GIB
zinc ion aqueous mrl(25); bourcier(100-350c)
A B C D E F
-56474.0 353.126 0.000000E+00 0.000000E+00 0.000000E+00 -49.4186
TMIN = 298.15 K TMAX = 623.15 K

ZN CL E-1 (AQ) SOURCE GIBBMRAQU DATA TYPE GIB
zncl+
A B C D E F
-209749. 2428.72 0.327721 -.117518E-03 0.632719E+07 -370.117
TMIN = 298.15 K TMAX = 623.15 K

ZN CL2 (AQ) SOURCE GIBBMRAQU DATA TYPE GIB
zncl2
A B C D E F
-.291747E+07 63311.6 17.4973 -.547003E-02 0.137571E+09 -10554.4
TMIN = 298.15 K TMAX = 623.15 K

ZN CL3 E1 (AQ) SOURCE GIBBMRAQU DATA TYPE GIB
zncl3-
A B C D E F
0.109189E+07 -28272.5 -7.91290 0.240315E-02 -.604332E+08 4739.00
TMIN = 298.15 K TMAX = 623.15 K

ZN CL4 E2 (AQ) SOURCE GIBBMRAQU DATA TYPE GIB
zncl4--
A B C D E F
0.775159E+07 -179938. -50.0473 0.153971E-01 -.390313E+09 30073.0
TMIN = 298.15 K TMAX = 623.15 K

ZN H2 S2 (AQ) SOURCE GIBBMRAQU DATA TYPE GIB
zn(hs)2
A B C D E F
830939. -22538.8 -6.76334 0.204619E-02 -.348692E+08 3830.02
TMIN = 298.15 K TMAX = 623.15 K

ZN O H2 S (AQ) SOURCE GIBBMRAQU DATA TYPE GIB
znoh(hs)
A B C D E F
0.275682E+07 -69244.1 -20.4729 0.646392E-02 -.128135E+09 11697.8
TMIN = 298.15 K TMAX = 623.15 K

PB E-2 (AQ) SOURCE GIBBMRAQU DATA TYPE GIB
lead ion aqu mrl exact refit
A B C D E F
3277.92 -99.7312 0.000000E+00 0.000000E+00 0.000000E+00 12.1434
TMIN = 298.15 K TMAX = 623.15 K

PB CL E-1 (AQ) SOURCE GIBBMRAQU DATA TYPE GIB
pbcl+
A B C D E F
-306135. 5990.65 1.75312 -.606013E-03 0.136008E+08 -1003.38
TMIN = 298.15 K TMAX = 573.15 K

PB CL3 E1 (AQ) SOURCE GIBBMRAQU DATA TYPE GIB
pbcl3-
A B C D E F
346155. -6070.76 0.424233 -.791914E-03 -.320802E+08 855.087
TMIN = 298.15 K TMAX = 573.15 K

PB CL4 E2 (AQ) SOURCE GIBBMRAQU DATA TYPE GIB
pbcl4--
A B C D E F
-.156228E+07 35575.5 11.7150 -.410382E-02 0.622625E+08 -6074.65
TMIN = 298.15 K TMAX = 573.15 K

PB H2 S2 (AQ) SOURCE GIBBMRAQU DATA TYPE GIB
pb(hs)2
A B C D E F
-.144678E+07 43131.2 16.3720 -.603140E-02 0.466363E+08 -7584.17
TMIN = 298.15 K TMAX = 573.15 K

SI O2 (1) SOURCE CPDMRLDAT DATA TYPE CPD
silicon dioxide quartz alpha beta

DHF(298) = -217700.0 CAL S(298) = 9.910 CAL /K
CP = 11.2200 + (0.820000E-02*T) + (0.000000E+00*T*T) + (-270000. /T/T)
TMAX = 848.00 K DH(TMAX) = 290.0 CAL
CP = 14.4100 + (0.194000E-02*T) + (0.000000E+00*T*T) + (0.000000E+00/T/T)
TMAX = 2000.00 K DH(TMAX) = 0.0 CAL

FE MG4 AL2 SI3 O18 H8 SOURCE CPDOWNDAT DATA TYPE CPD
chlorite solidsolution

DHF(298) = -2032043.2 CAL S(298) = 117.460 CAL /K
CP = 168.442 + (0.424320E-01*T) + (0.000000E+00*T*T) + (-.367400E+07/T/T)
TMAX = 673.15 K DH(TMAX) = 0.0 CAL

ca mg c2 o6 SOURCE CPDMRLDAT DATA TYPE CPD
calcium magnesium carbonate dolomite

DHF(298) = -556000.0 CAL S(298) = 37.090 CAL /K
CP = 37.3300 + (0.192400E-01*T) + (0.000000E+00*T*T) + (-516000. /T/T)
TMAX = 1200.00 K DH(TMAX) = 0.0 CAL

FE3 O4 SOURCE CPDMRLDAT DATA TYPE CPD
triiron tetroxide magnetite

DHF(298) = -267000.0 CAL S(298) = 34.930 CAL /K
CP = 38.2553 + (0.165333E-01*T) + (0.967239E-05*T*T) + (-713465. /T/T)
TMAX = 600.00 K DH(TMAX) = 0.0 CAL
CP = 1286.74 + (-2.49318 *T) + (0.143294E-02*T*T) + (-.926356E+08/T/T)
TMAX = 848.00 K DH(TMAX) = 0.0 CAL
CP = 48.0000 + (0.000000E+00*T) + (0.000000E+00*T*T) + (0.000000E+00/T/T)
TMAX = 1870.00 K DH(TMAX) = 33000.0 CAL
CP = 48.0000 + (0.000000E+00*T) + (0.000000E+00*T*T) + (0.000000E+00/T/T)
TMAX = 3000.00 K DH(TMAX) = 0.0 CAL

ZN S SOURCE CPDMRLDAT DATA TYPE CPD
zinc sulphide sphalerite

DHF(298) = -49000.0 CAL S(298) = 13.800 CAL /K
CP = 11.7700 + (0.126000E-02*T) + (0.000000E+00*T*T) + (-116000. /T/T)
TMAX = 1500.00 K DH(TMAX) = 0.0 CAL

pb S SOURCE CPDMRLDAT DATA TYPE CPD
lead sulphide solid liquid galena

DHF(298) = -23500.0 CAL S(298) = 21.800 CAL /K
CP = 11.1700 + (0.220000E-02*T) + (0.000000E+00*T*T) + (0.000000E+00/T/T)
TMAX = 1392.00 K DH(TMAX) = 8700.0 CAL
CP = 14.8000 + (0.000000E+00*T) + (0.000000E+00*T*T) + (0.000000E+00/T/T)
TMAX = 1800.00 K DH(TMAX) = 0.0 CAL

FE S2 SOURCE CPDMRLDAT DATA TYPE CPD
iron disulphide solid marcasite pyrite

DHF(298) = -41000.0 CAL S(298) = 12.650 CAL /K
CP = 17.8690 + (0.133300E-02*T) + (0.000000E+00*T*T) + (-304500. /T/T)
TMAX = 1016.00 K DH(TMAX) = 0.0 CAL

CA C O3 SOURCE CPDMRLDAT DATA TYPE CPD
calcium carbonate calcite

DHF(298) = -288568.0 CAL S(298) = 21.919 CAL /K
CP = 24.9800 + (0.524000E-02*T) + (0.000000E+00*T*T) + (-620000. /T/T)
TMAX = 1500.00 K DH(TMAX) = 0.0 CAL